Miniaturization and Characterization of Patient Derived Hepatocellular Carcinoma Tumor Organoid Cultures for Cancer Drug Discovery Applications

David A. Close , Paul A. Johnston

PII: S2472-5552(24)00063-7
DOI: https://doi.org/10.1016/j.slasd.2024.100201
Reference: SLASD 100201

To appear in: *SLAS Discovery*

Received date: 8 August 2024
Revised date: 5 December 2024
Accepted date: 8 December 2024

Please cite this article as: David A. Close , Paul A. Johnston , Miniaturization and Characterization of Patient Derived Hepatocellular Carcinoma Tumor Organoid Cultures for Cancer Drug Discovery Applications, *SLAS Discovery* (2024), doi: https://doi.org/10.1016/j.slasd.2024.100201

Title: Miniaturization and Characterization of Patient Derived Hepatocellular Carcinoma Tumor Organoid Cultures for Cancer Drug Discovery Applications.

David A. Close[1] and Paul A. Johnston[1,2, $].

1. Department of Pharmaceutical Sciences[2], School of Pharmacy, University of Pittsburgh, Pittsburgh, PA 15261, USA.
2. University of Pittsburgh Medical Center Hillman Cancer Center[3], Pittsburgh, PA 15232, USA.

$ Corresponding Author: Paul A. Johnston Ph.D., Professor, Department of Pharmaceutical Sciences, School of Pharmacy, Salk Hall Room 7402, 3501 Terrace Street, Pittsburgh PA 15261. Phone: (412) 383-6605, Email: pai18@pitt.edu

Author Contributions:

D.A.C. propagated organoid cultures, performed biological experiments, staining, drug screening, analyzed and interpreted data, and edited the manuscript. P.A.J. conceived and supervised the study, prepared, and wrote the manuscript.

Abstract

Patient derived tumor organoid (PDTO) models retain the structural, morphological, genetic, and clonal heterogeneity of the original tumors. The ability to efficiently generate, expand, and biobank PDTOs has the potential to make the clinical diversity of cancer accessible for personalized medicine assay guided therapeutic drug selection and drug discovery. We describe the miniaturization and growth in 96- and 384-well formats of a single non-tumor liver and two Hepatocellular carcinoma (HCC) organoids derived from cryopreserved PDTO cells and the application of high content imaging (HCI) to characterize the models and enhance drug sensitivity testing. Non-invasive sequentially acquired transmitted light images showed that seeding cryopreserved cells from non-tumoral and HCC PDTOs into 96- or 384-well plates in reduced growth factor Matrigel (rgf-MG) that were fed with growth medium every 3 days supported organoid growth up to 15 days. The number and sizes of organoids increased with longer times in culture. HCC PDTO's had more heterogeneous morphologies than non-tumor organoids with respect to size, shape, and optical density. Organoids cultured in rgf-MG could be stained *in situ* with HCI reagents without mechanical, chemical or enzymatic disruption of the hydrogel matrices and quantitative data extracted by image analysis. Hoechst and live/dead reagents provided organoid numbers and viability comparisons. HCC PDTO's stained with phalloidin or immuno-stained with α-tubulin antibodies revealed F-actin and microtubule cytoskeleton organization. HCC PDTO's stained with antibodies to signaling pathway proteins and their phosphorylation status allowed comparisons of relative expression levels and inference of pathway activation. Images of HCC PDTO's exposed to ellipticine showed that drugs penetrate Matrigel hydrogels and accumulate in organoid cells. 9-day 384-well HCC organoid cultures exhibited robust and reproducible growth signals suitable for cancer drug testing. Complimenting cell viability readouts with multiple HCI parameters including morphological features and dead cell staining improved the analysis of drug impact and

enhanced the value that could be extracted from these more physiologically relevant three-dimensional HCC organoid cultures.

Introduction.

Despite large investments in cancer research, drug discovery and development, new drug approval rates remain low ≤5% and advanced stage metastatic tumors incurable[1-3]. It has been proposed that incorporating more complex and physiologically relevant cellular models into early lead discovery will raise new cancer drug approval rates [4, 5]. For solid tumors like hepatocellular carcinoma (HCC), this would require three-dimensional (3D) *in vitro* tumor models that recapitulate human liver tumor architecture, heterogeneity, and biology[4, 5]. Individual patient derived 3D tumor organoid (PDTO) models are being utilized in precision medicine strategies for drug sensitivity testing to guide selection of cancer treatment options[6-16]. PDTO models address both inter- and intra-tumoral heterogeneity, and through expansion and biobanking of cells and cultures could provide platforms for drug discovery[6-12, 14-16]. PDTOs are produced by seeding dissociated patient derived tumor tissue cells into a semisolid extracellular matrix (ECM) such as Matrigel (MG), collagen, or ECM-inspired hydrogels and expanding these cells as 3D cultures[6-9, 11, 12]. PDTO models have been developed for several cancer types: colorectal, pancreas, breast, ovarian, stomach, prostate, sarcoma, glioblastoma multiforme, and mesothelioma[6-9, 11-13, 15]. PDTOs retain the structure, morphological, genetic, and clonal heterogeneity of the original tumor, and form tumors that resemble the tumor of origin when transplanted into mice [7, 8, 12, 14, 16]. The capability to create, expand, and biobank PDTOs of individual patients would make the clinical diversity of cancer accessible for chemo-sensitivity testing to guide therapeutic drug selection and for drug discovery[6, 7, 9, 11, 14-16]. We describe herein the miniaturization and HCI characterization of organoid cultures derived from cryopreserved HCC PDTOs for cancer drug sensitivity testing and potentially for future drug discovery efforts.

HCC accounts for >90% of primary liver cancers and is the 2nd leading cause of cancer related death with an annual worldwide incidence of ≥800,000 per year and the highest morbidity and mortality rates of any cancer worldwide[17-21]. HCC incidence is highest in China, Mongolia, southeast Asia, and sub-Saharan Africa, is ~2.4-fold more prevalent in males, and ~2-fold higher in non-Caucasians[17-21]. HCC incidence is rising in the USA and Europe, due to higher incidences of metabolic syndrome (obesity, insulin resistance, & dyslipidemia) and HCV infections[17-23]. In 2024, it is estimated there will be 41,630 new cases of HCC and 29,840 related deaths in the USA. HCC is associated with both infective and environmental etiologies including infection with hepatotropic viruses (HBV & HCV), non-alcoholic steatohepatitis (NASH), nonalcoholic fatty liver disease (NAFLD), alcohol and aflatoxin exposure which all contribute to liver pathogenesis[19, 20, 24-26]. Sequencing studies have revealed the highly complex genetic mutations and driver events involved in HCC tumorigenesis[25, 27]. On average, HCC tumors bear ~35-80 somatic mutations that activate or disrupt distinct molecular pathways in different HCC patients and the resulting heterogeneity contributes to the limited efficacy of existing therapies[25]. HCC therapeutic options are dictated by tumor stage, liver functionality, and patient performance status[18, 19]. Surgical resection, liver transplantation, and ablation offer high response rates with potential for cures for early stage HCC[18, 19]. However, due the asymptomatic nature of HCC, >80% of HCC patients are at an advanced stage by the time of clinical presentation[17-19, 28]. In the USA, 5-year survival rates for localized, regional, and distant stages of HCC are 37.3%, 13% and 3.3% respectively, with an overall 5-year survival of 21.7%. Systemic therapy is the only option for patients with inoperable advanced HCC. However, chemotherapy with cytotoxic agents or combinations of these drugs only elicit response rates of 10-20%, and fail to prolong HCC patient overall survival[18, 19]. Significant adverse events (AEs) associated with cytotoxic drugs limit HCC patient tolerance[18, 19]. Nexavar (sorafenib) a multi-tyrosine kinase inhibitor (TKI) was approved by the FDA for patients with advanced HCC and is the standard of care[18, 19, 24, 25, 29]. However, sorafenib improves overall survival by only ~3

months and elicits common AEs including diarrhea, weight loss, hand-foot skin reaction, and hypophosphatemia[18, 19, 29]. Stivarga (regorafenib), another multi-TKI was approved for HCC patients with tumors progressing on sorafenib, but only prolongs progression free survival by ~1.5 months and overall survival for ~3 months, with similar AEs to sorafenib[18, 30]. Despite the modest prolonged survival benefits of TKIs for patients with advanced HCC, several additional members of this drug class are in clinical development[18, 19]. Immune checkpoint immunotherapies are approved or in clinical development for advanced HCC[18]. Despite these myriad systemic therapy options, patients with inoperable advanced HCC typically survive <6 months, and the median survival of patients receiving therapy is only ~6-20 months[18, 19]. There remains therefore an urgent unmet clinical need for new and effective HCC therapies.

The complex etiologies, pathogenesis, and genetic heterogeneity of HCC makes drug discovery and development extremely challenging. PDTO models that can be sequenced to identify the specific genetic mutations and driver events in a patient's tumor and to provide drug sensitivity profiles to guide selection of cancer treatment options are being utilized in precision medicine anti-cancer strategies[6-16]. However, the efficiency of PDTO generation and whether sequencing and drug profiling data can be produced and analyzed in time to inform the selection of treatment options remain major challenges. Primary liver cancer (PLC) derived organoid cultures from HCC, cholangiocarcinoma (CC), and combined HCC/CC tumors preserve the histological architecture, gene expression, and genomic landscape of the original tumor[14]. In xenograft studies PLC-derived organoids demonstrated similar tumorigenic potential, histological features and metastatic properties to the parent tumor[14]. Drug sensitivity testing of 29 anticancer compounds in PLC organoids led to the identification of an ERK inhibitor as a potential therapeutic agent supporting personalized medicine applications for these cultures[14]. Similarly HCC organoid models derived from tumor needle biopsies preserved the morphology and genetic heterogeneity of the original tumors and exhibited differential drug sensitivities to sorafenib[16]. TP53 knockout in liver organoids generated from surgically excised non-tumor liver

tissues exhibited tumor like morphological changes including increased stemness and unrestricted *in vitro* propagation[31]. We describe here the miniaturization and growth in 96- and 384-well formats of a single non-tumor liver and two HCC organoid cultures derived from cryopreserved PDTO cells and the application of high content imaging (HCI) to characterize these 3D models and enhance the outcomes of drug sensitivity testing of a panel of TKI drugs.

Materials and Methods

Reagents

Formaldehyde (37%), N-acetyl-L-cysteine (NAC), Nicotinamide (NTA), human [Leu15]-Gastrin I, and the Y-27632 ROCK inhibitor were purchased from Sigma-Aldrich (St. Louis, MO). 99.9% high-performance liquid chromatography grade dimethyl sulfoxide (DMSO) were obtained from Alfa Aesar (Ward Hill, MA). Dulbecco's Mg^{2+}- and Ca^{2+}-free phosphate-buffered saline (PBS), AIM V medium, Insulin-Transferrin-Selenium (ITS), Minimal essential medium non-essential amino acids (MEM NEAA), B-27 supplement, fetal bovine serum (FBS), fungizone, 1X Penicillin-Streptomycin (P/S), and 1X L-Glutamine were all purchased from Gibco (Grand Island, NY). Collagenase type II was purchased from Worthington (Lakewood, NJ). Reduced growth factor Matrigel (rgf-MG) was purchased from Corning (Manassas, VA). Noggin, Epidermal Growth factor (EGF), Fibroblast Growth factor-10 (FGF-10), and Hepatocyte Growth Factor (HGF) were all purchased from Thermo Fisher Scientific (Waltham, MA). Forskolin and the TGF-β inhibitor A83-01 were purchased from Tocris (Minneapolis, MN). CellTiter-Blue® (CTB) was purchased from Promega Corporation (Madison, WI). Hoechst 33342, Calcein AM (CAM), Ethidium Homodimer (EtHD) and Texas Red-X Phalloidin were purchased from Life Technologies (Thermo Fisher Scientific, Waltham, MA). Rabbit anti-signaling pathway antibodies to Akt (# 9272), Src (# 2109), pSrc-Y527 (# 2105), and β-Catenin (# 8480) were purchased from Cell Signaling Technologies (Danvers, MA).

Hepatocellular carcinoma (HCC) Patient Derived Tumor Organoids (PDTO)

Cryopreserved single cell suspensions from established non-tumor and HCC PDTO cultures were kindly provided by Dr. Nathalie Wong in the Department of Surgery, Sir YK Pao Centre for Cancer, The Chinese University of Hong Kong, Shatin, Hong Kong, China[31]. Human HCC tumor and adjacent non-tumor liver tissues were collected from patients that underwent curative hepatectomy at the Prince of Wales Hospital, Hong Kong[31]. Informed consent was obtained from all recruited patients and the study procedure was approved by The Joint Chinese University of Hong Kong-New Territories East Cluster Clinical (CUHK-NTEC) Clinical Research Ethics Committee. Organoid cultures were established from excised HCC tumor and non-tumoral liver tissues as described previously[31]. Briefly, tissue samples were mechanically minced and enzymatically digested with 225 U/mL collagenase type II at 37°C for 15-30 mins, cell clusters were filtered through a 100 µm cell strainer and seeded at a cell density of $5x10^5$ live cells in 40 uL of rgf-MG[31]. Matrigel cell suspensions were solidified in a 37°C incubator for 15 mins prior to the addition of culture media. HCC organoids were cultured in basal medium consisting of AIM-V medium supplemented with 16% FBS, 1X P/S, 1X L-Glutamine, a 1:500 dilution of ITS, and 1% MEM NEAA[31]. Adjacent non-tumor liver organoids were additionally supplemented with 30% Wnt3a and 10% R-spondin-1 cell conditioned media, 2% B-27 supplement, 1% N2 supplement, 1 mM NAC, 10 mM NTA, 25 µg/mL Noggin, 50 ng/mL EGF, 100 ng/mL FGF-10, 25 ng/mL HGF, 10 nM human [Leu15]-Gastrin I, 10 µM Forskolin and the TGF-β inhibitor A83-01[31]. Cryopreserved cells from a non-tumor liver organoid culture that was established from non-tumor adjacent tissue excised from a 63-year-old patient with a primary HCC tumor was designated HCCorg-1N for Hepatocellular carcinoma (“HCC”) organoid (“org”) patient number 1 (“-1”) from non-tumoral adjacent (“N”) tissue. Cryopreserved cells from HCC PDTO cultures that were established from primary HCC tumor tissue excised from a 63-year-old female patient or from a 56-year-old male patient were designated HCCorg-1T and HCCorg-2T respectively.

Liver Organoid Maintenance: Recovery from freezing, Expansion in culture, and Passaging

Cryopreserved PDTO cell suspensions (around 1 x 10^5 cells/vial) were thawed and Matrigel cultures were typically first reestablished in 24-well plates. Cryovials of frozen dispersed PDTO cells removed from liquid nitrogen, were thawed at 37°C, and centrifuged at 2000 x RPM for 3 mins. Cell freezing medium was aspirated, pelleted cells were resuspended in 1 mL PBS, viable trypan blue excluding cells were counted on a hemocytometer, cells were centrifuged at 2000 rpm for 3 mins, and the PBS was carefully aspirated. Pelleted cells were resuspended in 100% rgf-MG maintained on ice at a density of 1 x 10^5 viable cells per 40 µL of rgf-MG and seeded into the centers of wells on a 24-well plate. The plate was carefully inverted and placed in a humidified incubator at 37°C with 5% CO_2 for 15 mins before the addition of 500 µL of growth medium. Growth media was exchanged twice weekly (Tuesdays and Fridays), by the removal of 300 µL of spent medium and replacement with 400 µL of fresh media respectively.

In 96-well plates, viable pelleted cells were resuspended in 100% rgf-MG maintained on ice at a density of 1.5 to 3 x 10^3 viable cells per 5 µL of Matrigel and 5 µL of cell suspension was seeded into the center of wells of a 96-well plate using a Matrix automated multichannel pipette (Thermo Fisher Scientific, Waltham, MA). 96-well plates were carefully inverted and placed in a humidified incubator at 37°C with 5% CO_2 for 15 mins to solidify before addition of 100 µL of growth medium. Growth media was exchanged twice weekly by the removal of 60 µL of spent medium and replacement with 70 µL of fresh media. The protocol for 384-well plates is described below in the growth monitoring and growth inhibition assay section.

When HCC and non-tumor organoid cultures were judged to be ~ 80% confluent by microscopic evaluation, they were passaged, typically at a 1:2 ratio early after breakout but at

higher ratios up to 1:5 after recovery. To dissociate MG cultures for passaging or cryopreservation, 50% of the spent medium was aspirated and the remaining media and MG disc were transferred into a sterile 1.5 mL microfuge tube, centrifuged for ~1 min, and the remaining medium was carefully aspirated. 500 µL of PBS was added and after mechanical disruption of the MG disc by repeated aspiration/dispensing pipetting cycles, the tube was centrifuged for ~1 min and the remaining medium carefully aspirated. The cell-MG pellet was resuspended in 500 µL of Accumax (Invitrogen) and incubated in a water bath at 37º C for 20 mins. Every 5 min the cell-MG mixture was mechanically disrupted using a Vortex and/or repeated aspiration/dispensing pipetting cycles. After 20 min the tube was centrifuged 2,000 RPM for 3 min, the supernatant was carefully aspirated, and the cells were resuspended in 1 mL of PBS. For cell passage, the cell suspension was centrifuged at 2,000 RPM for 3 min, the supernatant was carefully aspirated, and cells were resuspended in rgf-MG on ice before seeding into pre-warmed 24-, 96- or 384-well microtiter plates that were then inverted and solidified in 37°C incubator for 15 mins prior to the addition of growth media. For cells to be cryopreserved, the cell suspension was centrifuged at 2,000 RPM for 3 min, supernatant was carefully aspirated, and 1 x 10^5 viable cells were resuspended in 500 µL of freezing medium, placed in cryovials which were then frozen at -80ºC overnight and transferred to liquid Nitrogen for long term storage.

384-well Hepatocellular carcinoma Organoid Growth Monitoring and Growth Inhibition Assays.

To increase throughput and capacity and reduce the number of cells required for HCC organoid drug sensitivity screening we miniaturized organoid growth assays into 384-well format. To reduce the viscosity of the HCC organoid cell suspension and improve the ease of pipetting and liquid handling accuracy in 384-well plates, cells were resuspended in 75% rgf-MG. HCC organoids were dissociated into single cells with Accumax, viable trypan blue

excluding cells were counted on a hemocytometer and resuspended in cold 75% rgf-MG at 1500 cells per 15 µL. 15 µL of cells resuspended in 75% of rgf-MG were seeded into 384-well flat bottom plates using a Matrix automated multichannel pipette and the Matrigel was solidified in 37°C incubator for 15 mins prior to the addition of growth media to bring the final volume to 50 µL per well. On day 0 HCCorg-1T and HCCorg-2T cells were seeded at between 1,500 to 3,000 cells per well in 75% rgf-MG in 384-well plates; on day 3 HCC organoids were fed by automated media exchange; on day 6 HCC organoids were fed by automated media exchange and then compounds or controls were dispensed into wells at the indicated concentrations; on day 9 CTB was added to the wells and assay plates were returned the incubator for 4 h before the RFU (Ex. 560 nm/ Em. 590 nm) signals were captured on the M5e plate reader. On day 6, maximum control wells (Max, n=32) received 5 µL of DMSO (0.5% DMSO final) and minimum control wells (Min, n=32) received 5 µL of doxorubicin plus DMSO (200µM doxorubicin plus 0.5% DMSO final). Max and Min plate control wells represented uninhibited growth and 100% cytotoxicity respectively and were used to calculate assay performance statistics (S:B ratios and Z'-factor coefficients) and to normalize the data from compound treated wells as % inhibition of growth. Growth medium was exchanged by 3X aspiration and dispensing cycles on a Janus MDT automated liquid handling platform equipped with a 384-well dispensing head. Compounds and controls were dispensed into wells using the Janus MDT platform. We have routinely used CTB to quantify cell viability in 384-well 2D[32-35] and 3D (MCTS) [47-51] cancer cell line growth inhibition assays.

Liver Organoid Image Acquisition

12-Bit images of non-tumor and HCC liver organoids were acquired on an ImageXpress Micro (IXM) automated wide field HCI platform and analyzed with algorithms from the integrated MetaXpress Imaging and Analysis software (Molecular Devices LLC, Sunnyvale, CA) that were adapted from methods previously developed for head and neck cancer (HNC) cell line

multicellular tumor spheroid (MCTS) cultures[5, 36-40]. The IXM optical drive uses a 300 W Xenon lamp broad spectrum white light source and a 1.4-megapixel 2/3" chip Cooled CCD Camera and optical train for fluorescence and transmitted light phase contrast imaging. The IXM has Zero Pixel Shift (ZPS) filter sets: DAPI, FITC/ALEXA 488, CY3/TRITC, CY5, and Texas Red. Images of HCC PDTOs were sequentially acquired using either a 4X Plan Apo 0.20 NA or a 10X Plan Apo 0.30 NA objective in both the transmitted light (TL) and fluorescent image acquisition modes: DAPI, FITC, or Texas Red channels. We used the IXM automated image-based focus algorithm to acquire both a coarse focus (large µm steps) set of images of Hoechst-stained objects in the DAPI channel for the first organoids to be imaged, followed by a fine (small µm steps) set of images to select the best focus image. In subsequent wells and channels, only a fine focus set of images were acquired to select the best focus Z-plane. In some instances, a journal was used to acquire a Z-stack of images separated by defined Z-step intervals dependent upon the objective used which were then collapsed into a single maximum projection image. Organoid morphology and growth in 96-well and 384-well plates were assessed daily by acquiring multiple 4X or 10X TL images on the IXM to survey complete wells.

Liver Organoid Image Analysis

We used the multiwavelength cell scoring (MWCS) image analysis module to analyze 12-bit organoid fluorescent images adapted from a previous method used to analyze images of HNC MCTS cultures[5, 36-40]. To create a whole organoid mask, we set the approximate minimum width of the Hoechst-stained nuclei of the organoids to be 30 µm with an approximate maximum width to be 200 µm and applied a threshold intensity above local background of 250 grey levels. After applying user defined background average intensity thresholds, typically 300 and 200 grey levels above local background for the FITC and Texas Red channels respectfully, the MWCS module image segmentation created total organoid masks in all three fluorescent channels and quantified the mean average (MAFI) and integrated fluorescence intensity (MIFI) of the CAM

signal in the FITC channel and the EtHD signal in the Texas Red channel. MAFI and MIFI values represent the average and total pixel fluorescent intensities in channels 1, 2 or 3 within organoid masks of positively stained organoids above pre-set background thresholds.

Liver Organoid Live/Dead, Actin, Tubulin, and Signaling Pathway Staining

We used the Calcein AM (CAM) live cell and Ethidium Homodimer (EtHD) dead cell reagents to label viable and/or dead cells within liver organoid cultures, as described previously for HNC MCTS cultures[5, 36-40]. Organoid cultures were incubated with a cocktail of the Hoechst (8μg/mL), CAM (2.5μM), and EtHD (5μM) reagents for 1h, and DAPI, FITC and Texas Red channel images were sequentially acquired on the IXM using either a 4X or 10X objective in both the TL and fluorescent image acquisition modes.

To prepare organoid cultures in 96-well plates for actin, tubulin and signaling pathway staining *in situ*, cultures were first fixed and stained for 2 h with 3.7% formaldehyde containing 4 μg/mL Hoechst. The fixative was then aspirated and the fixed organoids were washed 3 x with 175 μL PBS and permeabilized overnight with 0.5% Triton X-100. Permeabilized organoids were then blocked for 60 minutes with either 1% BSA (phalloidin, pathway staining) or 0.1% Tween-20 (tubulin staining) in PBS before further processing. To stain organoids for F-actin, blocked samples were incubated with 75 μL of a 1:50 dilution of Texas Red-X Phalloidin in 1% BSA/PBS at 4°C for 16 h. Organoids were then washed 3 x with 175 μL PBS before 10X images were sequentially acquired on the IXM in the TL, DAPI, and Texas Red channels. To stain organoids for α-Tubulin, blocked samples were incubated with 75 μL of a 1:1000 dilution of primary α-Tubulin mouse monoclonal antibody (MAb) in 0.1% Tween-20/PBS at 4°C for 16 h. After 3 x 175 μL washes with PBS, organoids were incubated with a 1:1000 dilution of AlexaFluor-488 conjugated goat anti-mouse antibody for 2 h at room temperature. Organoids were then washed 3 x with 175 μL PBS before 10X images were sequentially acquired on the

IXM in the TL, DAPI, and FITC channels. To stain organoids for signaling pathway proteins by immunofluorescence, blocked samples were incubated with 75 µL of a 1:100 dilution of primary anti-target rabbit MAb in 0.1% Tween-20/PBS at 4°C for 16 h. After 3 x 175 µL washes with PBS, organoids were incubated with a 1:1000 dilution of AlexaFluor-594 conjugated goat anti-rabbit antibody for 2 h at room temperature. Organoids were then washed 3 x with 175 µL PBS before 10X images were sequentially acquired on the IXM in the TL, DAPI, and Texas Red channels.

Hepatocellular carcinoma Organoid Drug Penetration and Accumulation

Analysis of HCC organoid drug penetration and accumulation was performed as previously described for HNC MCTS cultures.[39] HCC organoids were seeded into and cultured in 96-well plates for 8 (HCCorg-2T) or 15 (HCCorg-1T) days in 75% Matrigel to allow organoids to grow out before a media exchange was performed and organoids cultures were then exposed to 10 µM ellipticine at 37°C, 5% CO_2, and 95% humidity for 1h prior to acquisition of 4X images on the IXM in the transmitted light and FITC channels. Individual transmitted light and FITC channel images are presented together with combined overlay images to illustrate ellipticine accumulation and distribution in HCC organoids.

Compounds and Compound Handling

To determine the GI_{50} concentrations of purchased tyrosine kinase inhibitors (TKIs), 10-point two-fold serial dilutions of test compounds in 100% DMSO were performed by using a 384-well P30 dispensing head on the Janus MDT Mini automated liquid handling platform (Perkin Elmer). Daughter plates containing 2 µL of serially diluted compounds in DMSO were prepared and replicated from the 384-well serial dilution master plates using the 384-well transfer head on the Janus MDT platform. Aluminum adhesive plate seals were applied, and plates were stored at −20°C. For testing in growth inhibition assays, daughter plates were

withdrawn from −20°C storage, thawed to ambient temperature, and centrifuged for 1 min at 100 g, and the plate seals were removed before the transfer of 38 µL of serum-free media (SFM) into wells by using a Matrix pipettor (Thermo Fisher Scientific, Waltham, MA), to generate intermediate stock concentrations of compounds. Diluted compounds were mixed by repeated aspiration and dispensation using the 384-well P30 head on the Janus MDT platform and then, 5 µL of diluted compounds was transferred to the wells of assay plates to provide the indicate final concentration response ranges with 0.5% DMSO final in the assay.

Data Processing and GI_{50}/IC_{50} Curve Fitting.

For HCC PDTO growth inhibition (GI_{50}) assays, the mean maximum DMSO control wells (Max controls n=32) and 200 µM doxorubicin mean minimum plate control wells (Min controls, n=32) were used to normalize the data from compound treated wells and to represent uninhibited growth and 100% cytotoxicity, respectively. The GI_{50} data were fit to a non-linear sigmoidal log (inhibitor) vs. normalized response variable slope model using the equation: Y=100/(1+10^((LogIC50-X) *Hillslope))), where Y was the percent growth inhibition and X was the corresponding log10 of the compound concentration. The GI_{50} is the concentration of compound that gives a 50% growth inhibition response, halfway between 0% and 100%. All curve fitting and graphs were created using the GraphPad Prism 10 software.

Results and Discussion

Recovery from freezing, Growth, and Morphologies of Non-tumor and Hepatocellular carcinoma Organoids Cultured in reduced growth factor Matrigel.

We wanted to assess the recovery, survival, growth, and morphologies of cryopreserved cells from established non-tumor liver organoids and HCC PDTOs that were thawed and resuspended in 100% rgf-MG and then seeded into 96-well plates and cultured in growth media (**Fig 1**). Non-tumor organoid HCCorg-1N cells were from organoids established from non-tumor adjacent liver tissue excised from a 63-year-old patient with a primary HCC tumor (**Fig 1A**),

while HCCorg-1T cells were from HCC PDTOs established from primary HCC tumor tissue excised from a 63-year-old female patient (**Fig 1B**), and HCCorg-2T cells were from HCC PDTOs established from primary HCC tumor tissue excised from a 56-year-old male patient (**Fig 1C**). HCCorg-1N at passage 4 (P4), HCCorg-1T at P9, and HCCorg-2T at P15 were seeded in 96-well plates at 2000-3000 cells/well in 100% rgf-MG and after solidifying the rgf-MG in a humified incubator at 37 °C, they were cultured with growth media and fed twice weekly by media exchange. Cultures were assessed daily for 15 days by acquiring 4 x 5 tiled 10X transmitted light (TL) images on the IXM to survey wells for organoid growth and morphology (**Fig 1**), like our analysis of HNC MCTSs[5, 36-40]. Tiled images covering the well together with single field of view (FOV) images are presented. For comparison, corresponding 10X and 20X images acquired on a stand-alone microscope when HCCorg-1N was originally established (P1) are presented, together with images of P14 and P11 of HCCorg-1T and HCCorg-2T respectively. To further illustrate the apparent heterogeneity of patient derived normal and tumor organoid cultures we present transmitted light FOV images of day 5 and day 15 HCCorg-1N P4, HCCorg-1T P9, and HCCorg-2T P15 cultures (**Fig 1D**).

After non-tumor and HCC organoid cells in 100% rgf-MG in 96-well plates were solidified in the incubator they form a disk that is thicker in the middle and thinner at the edges (**Fig 1**). The outlines of the rgf-MG disks were readily apparent in the HCC organoid cultures as early as day 6 and became more noticeable as the time in culture increased. The number and sizes of the non-tumor (**Fig 1A**) and HCC (**Fig 1B & 1C**) organoids increased with longer time in culture (**Fig 1D**). Although non-tumor HCCorg-1N containing wells exhibited fewer organoids (**Fig 1A & 1D**), their sizes increased steadily with time in culture such that organoids with diameters ~100 µm were observed as early as day 6, and organoids with diameters ≥200 µm were readily apparent on days 10 through 15. Organoid diameters were manually measured using the line scanning tool of the MetaXpress software. The predominant morphology of HCCorg-1N

organoids was a smooth circular structure with a saclike cavity surrounded by cells, consistent with an acinus-like structure (**Fig 1A & 1D**). In contrast the sizes, shapes, and morphologies of the HCC organoids were much more heterogeneous (**Fig 1B, 1C & 1D**). HCCorg-1T organoids were more numerous but generally smaller irregularly shaped multicellular organoids that were equally distributed between optically clear or dense organoids (**Fig 1B & 1D**). HCCorg-1T organoid sizes were very heterogenous but tended to be smaller with most being <100 µm by day 9 and ≤200 µm by day 15. HCCorg-2T organoids were generally larger more regularly shaped multicellular organoids that were mostly optically dense in appearance, less numerous than HCCorg-1T, but much more numerous than HCCorg-1N (**Fig 1C &1D**). The sizes of HCCorg-2T organoids were also very heterogeneous with many being ~100 µm by day 9 and ≥200 µm by day 15 (**Fig 1C &1D**). *In situ* non-invasive TL images sequentially acquired over time demonstrated that seeding dissociated cryopreserved cells isolated from established non-tumor liver organoid and HCC PDTOs into 100% rgf-MG with growth medium in 96-well plates can support the recovery, survival, and outgrowth of organoids for up to 15 days in culture. The number and sizes of non-tumor and PDTO derived organoids increased with longer times in culture, and while HCCorg-1N morphologies were more uniform and acinus-like, HCCorg-1T and HCCorg-2T organoids were heterogeneous with respect to size, shape, and optical appearance. Although, the MetaXpress image analysis software of the IXM platform does not contain algorithms to analyze transmitted light images, the images effectively convey the apparent heterogeneity of patient derived normal and tumor organoid cultures with respect to size, morphologies, and optical density (**Fig 1**).

Live/Dead Staining of Non-tumor and Hepatocellular carcinoma Organoids in Matrigel.

We wished to determine whether we could use Calcein AM (CAM) live cell and Ethidium Homodimer (EtHD) dead cell reagents to assess and compare the viability of non-tumor and HCC organoids cultured in 100% rgf-MG (**Fig 2**), as we have described previously for HNC

MCTSs[5, 36-40]. Full FOV (**Fig 2A**) and cropped (**Fig 2B**) 10X TL, Hoechst, CAM, EtHD, and live/dead color composite images of HCCorg-1N P4, HCCorg-1T P8, and HCCorg-2T P15 organoids cultured in 96-well plates for 10 days in rgf-MG and stained *in situ* are presented. The cropped images (**Fig 2B**) showcase one or two organoids selected from the full FOV images bounded by the yellow boxes (**Fig 2A**). By day 10, non-tumor liver organoid and HCC organoids exhibited strong CAM staining with little or no EtHD staining, indicating that the cells in the organoids were viable (**Fig 2A & 2B**). Consistent with **Fig 1A** non-tumor HCCorg-1N organoids formed large (150 µm) acinus-like smooth circular structures with a saclike cavity surrounded by cells (**Fig 2A & 2B**). Hoechst staining of HCCorg-1N organoids revealed the presence of stained nuclei within the cavity area apparent in the TL images and that the cells of organoids were strongly positive for CAM live cell staining with only background EtHD dead cell staining (**Fig 2A & 2B**). Also consistent with the TL images presented above (**Fig 1B & 1C**), HCCorg-1T and HCCorg-2T cells formed smaller (60-75 µm) heterogeneous and irregular shaped multicellular organoids that could be stained with Hoechst and were strongly positive for CAM live cell staining with only weak EtHD dead cell staining (**Fig 2A & 2B**). To see if we could quantify the total number of Hoechst stained organoids and compare the levels of live/dead staining in organoid cultures we modified a multiwavelength cell scoring (MWCS) image analysis module that we had previously used to analyze live/dead images of HNC MCTS cultures[5, 36-40]. To create a whole organoid mask, we set the approximate minimum width of the Hoechst-stained nuclei of the organoids to be 30 µm with an approximate maximum width to be 200 µm and applied a threshold intensity above local background of 250 grey levels (**Fig 2C**). We then applied background average intensity thresholds, typically 300 and 200 grey levels above local background, for the FITC and Texas Red channels respectfully, and the MWCS image segmentation created total organoid masks in all three fluorescent channels (**Fig 2C**) and used these masks to quantify the total number of Hoechst-stained organoids (**Fig 2D**) and the mean average (MAFI) (**Fig 2E**) and integrated (MIFI) (**Fig 2F**) fluorescence intensities of the

CAM and EtHD signals within the organoid masks for each channel. Consistent with the strongly positive CAM live cell staining and weak EtHD dead cell staining apparent in the images (**Fig 2A & 2B**), the mean average (**Fig 2E**) and integrated (**Fig 2F**) fluorescence intensities of the CAM signals were substantially higher than the corresponding EtHD signals. One limitation of this approach is that not all the organoids in the rgf-MG cultures occupy the same Z-plane and therefore not all the fluorescent signals in the 3 channels are sharply in focus. In instances where we acquired Z-stacks of images separated by defined Z-step intervals, collapsing the image stack into a single maximum projection image did not appear to substantially improve the out of focus signals limitation (data not shown). Even though we set thresholds over background low enough to capture the more diffuse signals, this likely contributes to the variability apparent in the data, especially in the mean integrated intensity values of the CAM signals (**Fig 2F**). Never-the-less, these data indicate that non-tumor and HCC organoids cultured in rgf-MG can be stained *in situ* with live/dead reagents and image analysis used to quantify and compare the numbers and relative viabilities of organoids.

Cytoskeleton and Signaling Pathway Protein Staining of Hepatocellular carcinoma Organoids in Matrigel.

To determine whether we could stain the cytoskeletons of HCC organoids cultured in 100% rgf-MG *in situ*, we incubated fixed and permeabilized organoids with Phalloidin conjugated with Texas Red to stain F-actin (**Fig 3A & 3B**) or with anti-α-Tubulin primary antibodies and FITC conjugated secondary antibodies to visualize microtubules (**Fig 3C**). Full FOV (**Fig 3A**) and cropped (**Fig 3B**) 10X TL, Hoechst, Phalloidin, and DNA/F-actin color combined images of HCCorg-1T and HCCorg-2T organoids cultured in 100% rgf-MG in 96-well plates for 10 days are presented. Phalloidin efficiently penetrated and stained the F-actin cytoskeletons of both the more numerous and smaller (≤100 μM) HCCorg-1T organoids as well as the fewer but larger (≥100 μM) HCCorg-2T organoids cultured in rgf-MG. The cropped images of HCCorg-1T

and HCCorg-2T organoids illustrate the heterogeneity of F-actin staining patterns (**Fig 3B**). The MWSC scoring whole organoid image analysis algorithm provided quantitative data for the number of Hoechst-stained HCCorg-1T and HCCorg-2T organoids analyzed (**Fig 3D**) and the relative average (**Fig 3E**) and integrated (**Fig 3F**) fluorescent intensities of the phalloidin-stained F-actin signals. For the anti-α-Tubulin antibody staining of organoid cultures we increased the length of incubation with both the primary and secondary antibodies to 16-18 h and 2 h respectively. To quantify the total numbers of Hoechst stained organoids and compare the levels of anti-α-Tubulin antibody staining (**Fig 3G, 3H & 3I**) in organoid cultures we applied the same MWCS image analysis procedure. To create a whole organoid mask, we set the approximate minimum width of the Hoechst-stained nuclei of the organoids to be 30 µm with an approximate maximum width to be 300 µm and applied a threshold intensity above local background of 75 grey levels above local background. We then applied background average intensity thresholds, typically 50 and 250 grey levels above local background, for the FITC (α-Tubulin) and Texas Red channels (phalloidin/F-actin) respectfully, to create total organoid masks in both channels. We used these masks to quantify the total number of Hoechst-stained organoids (**Fig 3D & 3G**) and the mean average (**Fig 3E & 3H**) and integrated (**Fig 3F & 3I**) fluorescence intensities of the phalloidin-stained F-actin and anti-α-Tubulin antibody stained microtubules within the organoid masks. Full FOV and cropped 10X TL, Hoechst, FITC (anti-α-Tubulin), and DNA/α-Tubulin color combined images of HCCorg-1T and HCCorg-2T organoids cultured for 10 days in 100% rgf-MG in 96-well plates are presented (**Fig 3C**). The MWCS whole organoid image analysis algorithm provided quantitative data for the number of Hoechst-stained HCCorg-1T and HCCorg-2T organoids analyzed (**Fig 3G**) and the relative average (**Fig 3H**) and integrated (**Fig 3I**) fluorescent intensities of the anti-α-Tubulin antibody stained microtubule signals. Although there was apparent microtubule staining in both HCCorg-1T and HCCorg-2T cultures (**Fig 3C, 3G, 3H, & 3I**), the staining intensity appeared stronger at the edges of some organoids perhaps suggesting that antibody penetration in fixed and

permeabilized organoids in rgf-MG was incomplete. Interestingly, microtubule staining of multicellular protrusions extending away from the main body of HCCorg-2T organoids by anti-α-Tubulin antibodies was strong (**Fig 3C**) whereas the staining of F-actin in similar structures by phalloidin were barely over background (**Fig 3B**). Figure 3 shows that HCC organoids cultured in 100% rgf-MG that have been fixed and permeabilized can be effectively stained *in situ* by fluorescent probes or antibodies to visualize the assembly and organization of their F-actin or microtubule cytoskeletons.

Encouraged by the ability to immuno-stain microtubules in HCC organoids (**Fig 3C, 3G, 3H, & 3I**), we explored whether we could also immuno-stain the proteins of key signaling pathways that are frequently altered in HCC; WNT/β-catenin, PI3K/Akt/mTOR, and SRC kinase pathways (**Fig 4**)[41-44]. Established HCCorg-2T organoids that had been cultured in 100% rgf-MG in 96-well plates were fixed in 4% paraformaldehyde and then permeabilized with 1% Triton X-100 before they were incubated overnight with a 1:100 dilution of primary antibodies to Akt, Src, pSrc-Y527, or β-Catenin (**Fig** 4). Goat anti-rabbit secondary antibodies conjugated with Texas Red were used to visualize primary antibody detection. Full FOV and cropped, indicated by the yellow bounding boxes, 10X TL, Hoechst (blue), Texas Red (Akt, Src, pSrc-Y527, or β-Catenin, red), and DNA/signaling protein color combined images of HCCorg-2T organoids are presented (**Fig 4A**). The images showed strong endogenous immuno-staining of total Akt, Src and β-Catenin expression in HCCorg-2T organoids but relatively low pSRC-Y527 staining (**Fig 4A**). We used the MWCS image analysis module to quantify the number of Hoechst-stained organoids (**Fig 4B**) and the MAFI values of their Hoechst DNA (**Fig 4C**) and signaling protein antibody staining levels (**Fig 4D**). Although 25% fewer HCCorg-2T organoids (291) stained with the pSRC-Y527 antibody were analyzed than with the Akt, Src and β-Catenin antibodies (≥400), all four groups exhibited comparable Hoechst MAFI values (**Fig 4B & 4C**). Although the MAFI values for Akt, Src, and β-Catenin antibody staining were between 1-5- to 1.9-fold higher than for pSrc-Y527 (**Fig 4D**), the differences were not statistically significant, likely because not all

the HCC organoids occupied the same Z plane and were in focus. Never-the-less, the data illustrate that HCC organoids cultured in 100% rgf-MG can be stained *in situ* with specific signaling pathway protein and phospho-specific antibodies that could be used to determine their relative expression levels and to infer pathway activation based on phosphorylation status. Furthermore, the data presented in Figures 3 (**Fig 3C, 3G, 3H, & 3I**) and 4 (**Fig 4A, 4B, 4C & 4D**) illustrate that PDTO cultures embedded in rgf-MG can effectively be fixed, permeabilized, and stained with antibodies *in* situ without prior disruption of the hydrogel matrix by mechanical, chemical, or enzymatic procedures. It's possible that the reproducibility of the antibody staining in PDTO cultures could be improved using microfluidic systems, which might improve the consistency of washing steps and antibody distribution. Similarly, magnetic manipulation of organoids isolated after disruption of the hydrogel matrix might also improve organoid handling during antibody staining and reduce variability.

Cancer Drug Penetration and Accumulation in Hepatocellular carcinoma Organoids in Matrigel.

Cells in solid tumors and 3D cultures experience adhesive, topographical, and mechanical cues that can alter their fundamental biology and responses to stimuli.[10-14, 19-26] Tumor cell packing densities and adhesion junctions between adjacent cells and with the ECM constitute permeability barriers that can restrict cancer drug penetration, distribution, and efficacy.[45-50] The physiochemical properties of drugs also affect tissue distribution, and cells that are distal to blood vessels in solid tumors experience lower concentrations due to limited drug penetration.[45, 46, 49] Reduced drug penetration in solid tumors contributes to the resistance towards numerous chemotherapeutic agents[27-29, 44-54]. In addition to potential drug permeability barriers due to the cell-cell, cell-ECM, and cell-Matrigel contacts that the cells in 3D organoids engage in, drugs must also penetrate the Matrigel hydrogel. We have previously used the fluorescent properties of anthracycline chemotherapeutics (idarubicin, daunorubicin, & doxorubicin) and ellipticine

taken up by cells to study drug penetration and accumulation in 2D and 3D MCTS cultures of HNC cell lines[37, 39]. The dimethyl-pyrido-carbazole plant alkaloid ellipticine inhibits topoisomerase II activity by DNA intercalation and exhibits antiproliferative activity against many human cancer lines, and towards murine and human leukemias *in vivo*[39, 51]. Although ellipticine in solution does not exhibit an obvious absorption peak or fluorescent emission spectrum when excited at 480 nm, when taken up by cells in 2D and 3D MCTS cultures exposed to ellipticine in the 1.56–25 µM range it produces strong fluorescence signals in FITC channel images[39, 52, 53]. To determine whether dispensing anti-cancer drugs into the media overlying HCC organoids cultured in rgf-MG is an effective drug exposure strategy, established HCCorg-1T and HCCorg-2T organoids that had been cultured in 75% rgf-MG in 96-well plates for 15 and 8 days respectively were exposed to 10 µM ellipticine in an incubator for 1 h at 37 °C, 5% CO_2, and 95% humidity. 4 x 4 tiled 4X TL and FITC images of live organoid cultures were then acquired on the IXM to survey the wells for ellipticine accumulation (**Fig 5**). Tiled TL and FITC images covering the well (**Fig 5A**) together with single 4X FOV images (**Fig 5B**) outlined by the yellow bounding box in the tiled images are presented. We used the MWCS image analysis whole organoid mask procedure to quantify the number of PDTO's (**Fig 5C**) and the average (**Fig 5D**) and integrated (**Fig 5E**) fluorescent intensities of the ellipticine signals in HCCorg-1T and HCCorg-2T organoids. We applied a threshold intensity above local background of 50 grey levels in the FITC (ellipticine) channel to create the organoid masks and quantify ellipticine accumulation. While it is apparent from the tiled TL and FITC images that not all the HCC organoids were in the same focal plane and sharply in focus (**Fig 5A**), the TL-FITC channel overlays of the FOV images (**Fig 5B**) indicate that ellipticine fluorescence was restricted to and colocalized within HCCorg-1T and HCCorg-2T organoids as indicated by the average (**Fig 5D**) and integrated (**Fig 5E**) fluorescent intensity values. The accumulation and increased fluorescence of ellipticine in HCC organoids cultured in rgf-MG (**Fig 5**) indicate that dispensing

anti-cancer drugs into the media overlying organoid cultures in rgf-MG is an effective method of drug exposure.

384-well Hepatocellular carcinoma Organoid Growth and Growth Inhibition Assays in Matrigel.

To enhance throughput and capacity and reduce the number of cells required for HCC organoid drug sensitivity screening we miniaturized organoid growth assays into 384-well format (**Fig 6**). We used 75% rgf-MG for the 384-well format HCC organoid growth assays to improve the ease of pipetting and liquid handling accuracy by reducing the viscosity of the HCC organoid cell suspension. HCCorg-1T and HCCorg-2T cells were seeded at 1,500 and 2,000 cells per well in 15 µL of 75% rgf-MG and single 4X TL FOV images were acquired every 3 days and these images are presented together with larger cropped images indicated by the yellow bounding box (**Fig 6A**). Consistent with HCCorg-1T and HCCorg-2T cells cultured in 100% rgf-MG in 96-well plates (**Fig 1B & 1C**), the number and sizes of the organoids increased with longer times in culture in 75% rgf-MG in 384-well plates (**Fig 6A**). The organoids were heterogenous with respect to numbers, sizes, shapes, and morphologies, although HCCorg-1T organoids were typically more numerous and smaller than HCCorg-2T organoids (**Fig 6A**). To determine whether HCC organoids would be compatible with 384-well growth assays we conducted cell titer blue (CTB) cell seeding density and time course experiments to select 384-well seeding densities that allowed for active proliferation throughout a 12 day culture period (**Fig 6B & 6C**). On day 0, 384-well CTB RFU signals were linear with respect to the number of viable HCCorg-1T (r^2= 0.94) and HCCorg-2T (r^2= 0.89) cells seeded per well (**Fig 6B**). At equivalent seeding densities, ranging from 250 up to 2000 cells per well, HCCorg-2T cells were much more efficient than HCCorg-1T cells at converting CTB resazurin to fluorescent resorufin, perhaps indicating they are more metabolically active. In time course experiments, HCC organoid CTB signals were captured every 3 days in culture (**Fig 6C**). HCCorg-1T and HCCorg-

2T cells seeded in 75% rgf-MG in 384-well plates at 1,500 or 2,000 cells per well and cultured for 12 days with automated media exchange every 3 days grew exponentially with doubling times of 3.7 (r^2= 0.87) and 5.6 (r^2= 0.85) days respectfully (**Fig 6C**).

Maximum control wells (Max, n=32) received 5 µL of DMSO (0.5% DMSO final) and minimum control wells (Min, n=32) received 5 µL of doxorubicin plus DMSO (200µM doxorubicin plus 0.5% DMSO final) and represented uninhibited growth and 100% cytotoxicity respectively. Max and min plate controls were used to calculate assay performance statistics (**Fig 6D & 6F**) and to normalize the data from compound treated wells as % inhibition of growth (**Fig 6E & 6G**). HCCorg-1T cells seeded at 1,500 cells per well produced a signal to background ratio (S:B ratio) of 3.7-fold and Z'-factor coefficient of 0.65, while HCCorg-2T cells seeded at 2,000 cells per well produced a S:B ratio of 7.3-fold and Z'-factor coefficient of 0.90 (**Fig 6D & 6F**), indicating that both HCC organoid growth assays were robust and reproducible. Normalized growth inhibition curves for HCCorg-1T and HCCorg-2T organoids and the corresponding GI_{50} values for doxorubicin and four TKIs are shown (**Fig 6E & 6G, & Table 1**). The curve fits (r^2) were slightly better for HCCorg-1T than HCCorg-2T PDTOs. Nilotinib failed to inhibit the growth of both HCC organoids at concentrations ≤ 200 µM, while Nexavar (sorafenib) only inhibited the growth (GI_{50} 75 µM) of HCCorg-1T organoids (**Fig 6E & 6G, & Table 1**). Dasatinib inhibited the growth of both HCCorg-1T and HCCorg-2T organoids with GI_{50}s of 53 and 59 µM respectively (**Fig 6E & 6G,** & **Table 1**). Crizotinib was the most potent TKI with GI_{50}s of 4 and 0.3 µM for HCCorg-1T and HCCorg-2T respectively. The cytotoxic chemotherapeutic doxorubicin was also potent with GI_{50}s of 0.45 and 3.6 µM for HCCorg-1T and HCCorg-2T respectively (**Fig 6E & 6G, & Table 1**). While it would have been informative to include the HCCorg-1N organoids in the anti-cancer drug growth inhibition studies, the growth media for the normal organoid cultures require several supplements to the basal media utilized for PDTO cultures and normal cultures only maintain a proliferative phenotype through a limited number (2-3) of passages.

Multiparametric Hepatocellular carcinoma Organoid Growth Inhibition Assays in Matrigel.

Relying solely on cell viability measurements such as CTB and/or CAM has been shown to under-estimate the impact of cancer drug exposure in MCTS cultures[38, 54]. Incorporating morphological changes and drug-induced increases in EtHD dead cell staining more than doubled the number of drugs that were considered to have substantially affected HNC MCTS cultures[38]. Cumulative multi-parameter drug impact analyses enable drug responses to be stratified into high, intermediate and low impact tiers[38, 54]. We conducted additional 384-well growth inhibition assays in HCCorg-2T organoids to evaluate the effects of 72 h exposure to the TKIs sunitinib, crizotinib, nexavar, and imatinib (**Fig 7 & Table 2**). Compound treated HCCorg-2T organoids were stained with a cocktail of Hoechst, CAM and EtHD and TL, DAPI, FITC and Texas Red channel images were acquired on the IXM (**Fig 7A**). Whole well montage images of the TL and DAPI channels together with color combined FITC (CAM, live, green) plus Texas Red (EtHD, dead, red) channels at six TKI concentrations, ranging from 9 up to 300 µM, plus DMSO controls are presented (**Fig 7A**). Compared to TL images of DMSO control wells, there was an apparent decrease in the number of organoids at the top 3-4 concentrations of sunitinib, crizotinib and nexavar, that was not apparent with imatinib exposure even at 150 µM (**Fig 7A**). There was a corresponding noticeable decrease in the number of Hoechst-stained organoids at the top 3-4 concentrations of sunitinib and crizotinib compared to DMSO control well DAPI images (**Fig 7A**). Indeed, the top 3 concentrations of sunitinib were devoid of Hoechst-stained organoids. Higher concentrations of crizotinib and nexavar produced DAPI images with a more diffuse background staining pattern, and nexavar also produced an intense punctate staining pattern (**Fig 7A**). DAPI staining images of imatinib treated cultures were very similar to those from DMSO controls. Based on CTB viability measurements normalized to Max (DMSO) and Min (doxorubicin) plate controls the calculated GI_{50}s for sunitinib, crizotinib, and nexavar were 65.2, 43.7 and 64.6 µM respectively, while imatinib apparently failed to inhibit HCCorg-2T

organoid growth at ≤300 µM (**Fig 7B & Table 2**). The MWCS image analysis module was then used to quantify the number of Hoechst-stained organoids (**Fig 7C**) and their mean integrated CAM (**Fig 7D**) and EtHD (**Fig 7E**) fluorescence intensities (MIFI). Based on the number of Hoechst-stained organoids the calculated GI_{50}s for sunitinib and crizotinib were 29.5 and 80.6 µM respectively, whereas both nexavar and imatinib failed to reduce Hoechst-stained organoid numbers at ≤300 µM (**Fig 7C & Table 2**). Compared to live/dead images of DMSO control wells all four TKIs produced a concentration dependent decrease in CAM live staining with a corresponding increase in EtHD dead staining (**Fig 7A**). Based on the MIFI signals of CAM live cell staining the calculated GI_{50}s for sunitinib, nexavar and imatinib were 19.5, 37.1 and 79 µM respectively (**Fig 7D & Table 2**). A GI_{50} could not be calculated for crizotinib from the CAM MIFI signals because they were suppressed by >50% at all concentrations tested (**Fig 7A & 7D**). Based on the MIFI signals of EtHD dead cell staining the calculated EC_{50}s for nexavar and imatinib were 17.7 and 66.2 µM respectively (**Fig 7E & Table 2**). EtHD dead cell staining EC_{50}s could not be calculated for either sunitinib or crizotinib because few organoids remained to be stained after 72 h at the top 3-4 compound concentrations, as indicated by the corresponding TL and DAPI images (**Fig 7A**). At sunitinib and crizotinib concentrations of 9 and 19 µM however, increased EtHD staining was apparent (**Fig 7A**). Based on a cumulative multi-parameter drug impact scoring strategy[38, 54], sunitinib, crizotinib, and nexavar would be considered high impact agents. The apparent failure of nexavar to effectively reduce Hoechst-stained organoid numbers at ≤300 µM (**Fig 7C & Table 2**) may be due to compound autofluorescence interference in the DAPI channel (**Fig 7A**). Based on CTB signals, TL images, and the number of Hoechst-stained organoid data, we would conclude that imatinib was ineffective against HCCorg-2T organoids at ≤300 µM. However, the live/dead images and corresponding quantitative data (**Fig 7A, 7D and 7E**) indicate that imatinib had a measurable effect on HCCorg-2T viability and should therefore be considered a low impact drug rather than ineffective. Similar to MCTS models[38, 54], incorporating multiple parameters like morphological

features and dead cell staining to compliment viability readouts improved the analysis of drug outcomes in organoid cultures and increased the number of drugs that were considered to have inhibited growth.

Conclusions.

PDTO models reportedly retain the structural, morphological, genetic, and clonal heterogeneity (inter- and intra-tumoral) of the original tumor and can form tumors that resemble the tumor of origin when transplanted into mice[6-12, 14-16]. The ability to efficiently generate, expand, and biobank PDTOs from individual patients has the potential to make the clinical diversity of cancer accessible for assay guided therapeutic drug selection and perhaps also drug discovery[6, 7, 9, 11, 14-16]. Non-invasive sequentially acquired TL images showed that seeding dissociated cryopreserved cells from previously established non-tumor liver organoid and HCC PDTO cultures into 96- or 384-well plates in rgf-MG fed with growth medium every 3 days supported organoid growth for up to 15 days. While the number and sizes of organoids increased with longer times in culture, HCC organoid morphologies were more heterogeneous than non-tumor cultures with respect to size, shape, and optical density. Organoids cultured in rgf-MG cultures could be stained *in situ* with Hoechst and live/dead reagents and HCI analysis methods provided quantitative readouts of the number and relative viability of organoids. Images of HCC PDTO rgf-MG cultures stained *in situ* with phalloidin or immuno-stained with α-tubulin antibodies provided visualizations of F-actin and microtubule cytoskeleton organization. Similarly, HCC organoids in rgf-MG cultures stained *in situ* with specific antibodies to signaling pathway proteins enabled comparisons of relative expression levels and inference of pathway activation based on their phosphorylation status. The accumulation and increased fluorescence of ellipticine in HCC organoids cultured in rgf-MG indicated that drugs penetrate the Matrigel hydrogel and achieve exposure. 9-day 384-well HCC organoid cultures exhibited robust and reproducible growth amenable to drug induced growth inhibition assays. Complimenting HCC organoid cell viability readouts with multiple HCI parameters like morphological features and

dead cell staining improved the analysis of drug impact and maximized the value that could be extracted from these more physiologically relevant 3D tumor cultures.

Funding: The studies reported herein were funded in part by grant support from the National Institutes of Health (NIH) R01CA229836 Johnston (PI) from the National Cancer Institute (NCI).

Acknowledgements: The authors would like to thank and acknowledge Dr. Nathalie Wong and Dr Alissa Wong both in the Department of Surgery, Sir YK Pao Centre for Cancer, The Chinese University of Hong Kong, Shatin, Hong Kong, China. Dr. Nathalie Wong provided the cryopreserved single cell suspensions from established non-tumor and HCC PDTO cultures and Dr. Alissa Wong provided technical guidance in their maintenance, handling and growth as organoid cultures.

Abbreviations: Hepatocellular carcinoma (HCC), three-dimensional (3D), patient derived tumor organoids (PDTOs), extracellular matrix (ECM), Matrigel (MG), reduced growth factor Matrigel (rgf-MG), hepatitis B virus (HBV), hepatitis C virus (HCV), non-alcoholic steatohepatitis (NASH), nonalcoholic fatty liver disease (NAFLD), adverse events (AEs), tyrosine kinase inhibitor (TKI), monoclonal antibody (MAb), Whole-genome sequencing (WGS), N-acetyl-L-cysteine (NAC), Nicotinamide (NTA), dimethyl sulfoxide (DMSO), Dulbecco's Mg^{2+}- and Ca^{2+}-free phosphate-buffered saline (PBS), Minimal essential medium non-essential amino acids (MEM NEAA), fetal bovine serum (FBS), Penicillin-Streptomycin (P/S), Epidermal Growth factor (EGF), Fibroblast Growth factor-10 (FGF-10), Hepatocyte Growth Factor (HGF), Cell Titer-Blue® (CTB) Calcein AM (CAM), Ethidium Homodimer (EtHD), High Content Imaging (HCI), ImageXpress Micro high content imaging platform (IXM), multiwavelength cell scoring image analysis module (MWCS), Zero Pixel Shift filter sets (ZPS), transmitted light (TL), field of view (FOV), head and neck cancer (HNC), multicellular tumor spheroids (MCTSs), relative florescent intensity units (RFUs),

mean average fluorescence intensity (MAFI), mean integrated fluorescence intensity (MIFI), concentration of compound that gives a 50% growth inhibition response halfway between 0% and 100% (GI_{50}), concentration of compound that gives a 50% increase in response halfway between 0% and 100% (EC_{50}), standard deviation of the mean (sd), not applicable (NA), not calculable (NC), maximum control wells (Max), minimum control wells (Min), signal to background ratio (S:B ratio).

Figure Legends

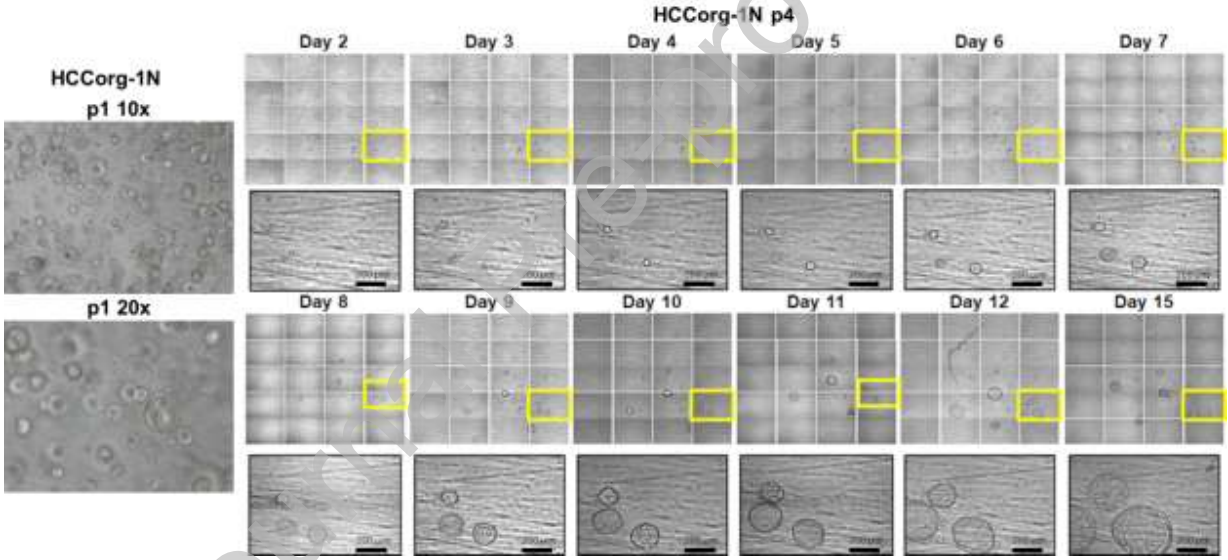

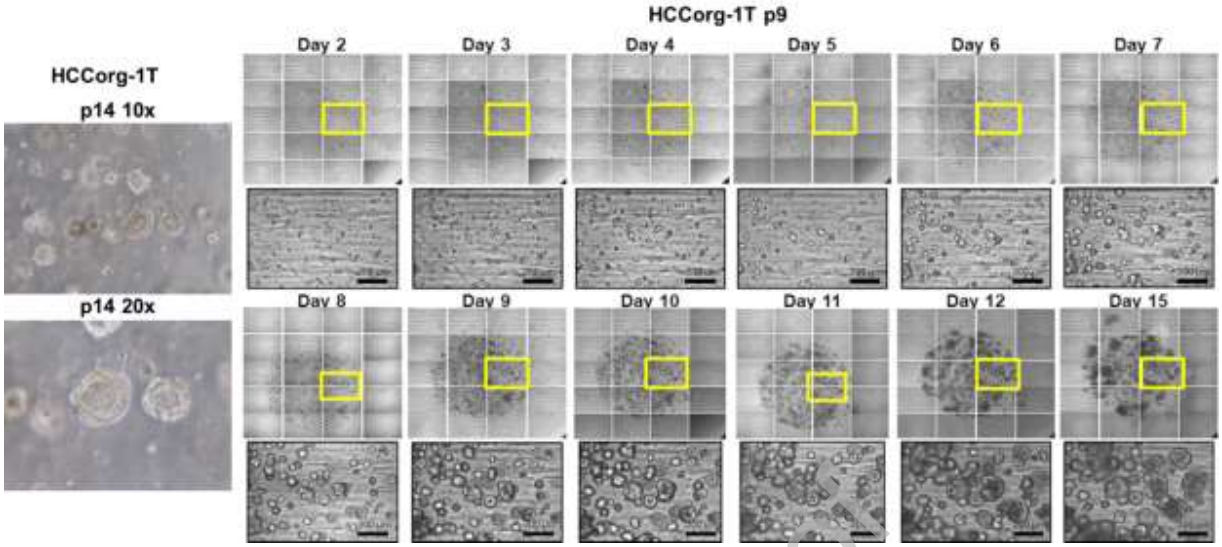

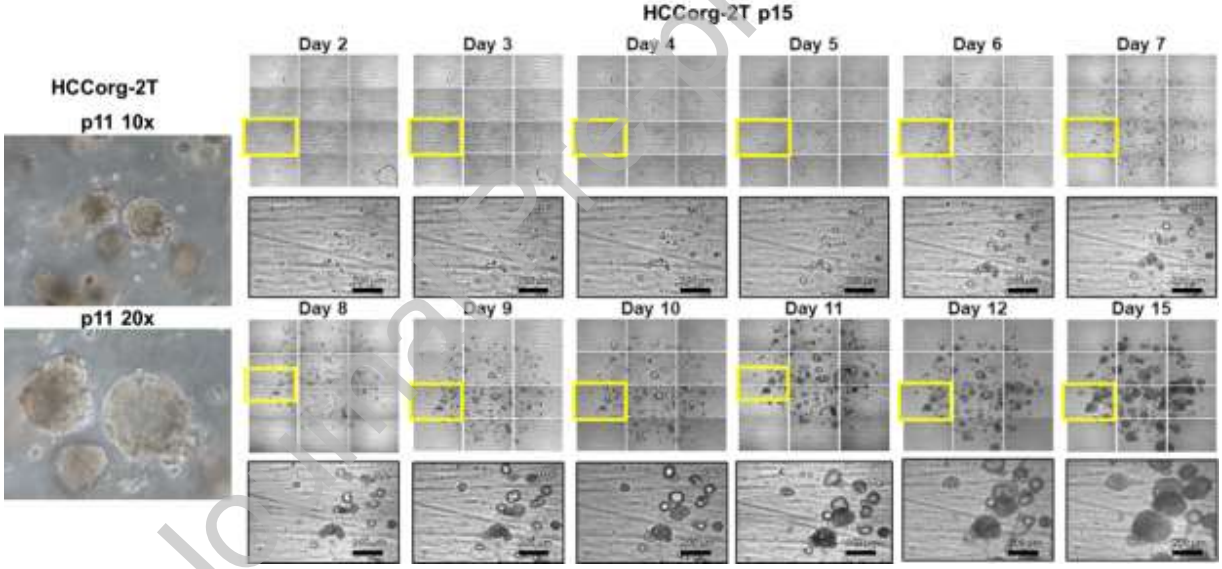

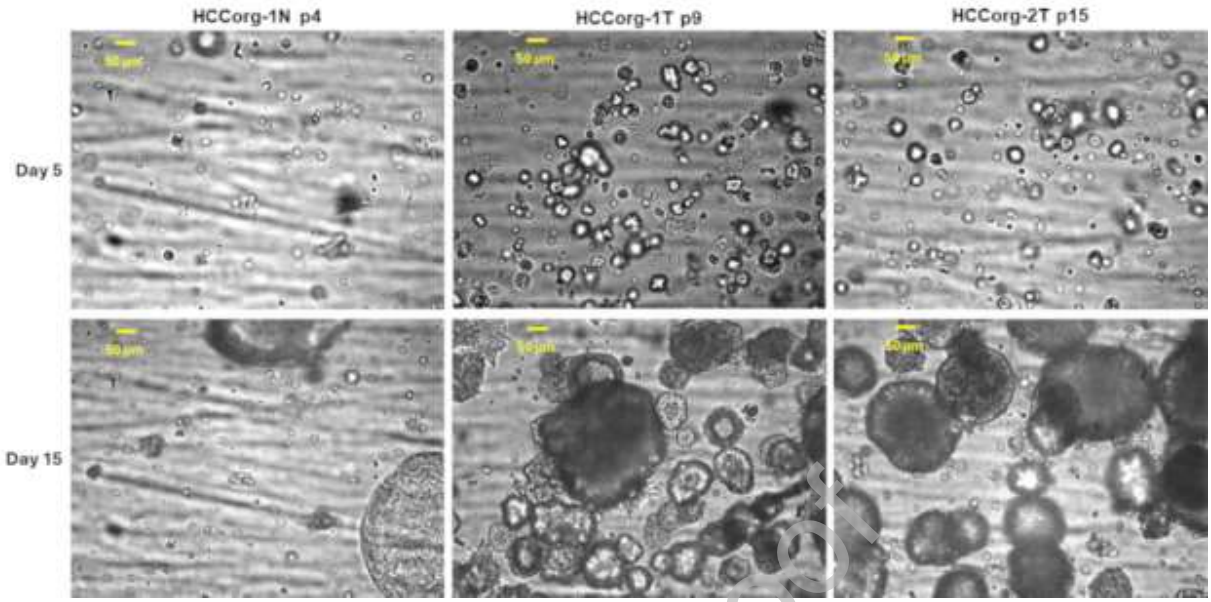

Figure 1. Sequentially Acquired Transmitted Light Images to Monitor the Growth and Morphologies of HCCorg-1N Non-tumor and HCCorg-1T and HCCorg-2T Hepatocellular Carcinoma Organoids cultured in Reduced Growth Factor Matrigel; A) HCCorg-1N Non-tumor Liver Organoids, B) HCCorg-1T HCC organoids, C) HCCorg-2T HCC Organoids, and D) Field of View images of day 5 and day 15 HCCorg-1N P4, HCCorg-1T P9, and HCCorg-2T P15 cultures. Cryopreserved HCCorg-1N cells were from a non-tumor liver organoid culture that was established from non-tumor adjacent tissue excised from a 63-year-old patient with a primary HCC tumor (**A**). Cryopreserved HCCorg-1T cells were from HCC PDTO cultures that were established from primary HCC tumor tissue excised from a 63-year-old female patient (**B**). Cryopreserved HCCorg-2T cells were from HCC PDTO cultures that were established from primary HCC tumor tissue excised from a 56-year-old male patient (**C**). HCCorg-1N P4, HCCorg-1T P9, and HCCorg-2T P15 cryopreserved cells were thawed and seeded into 96-well plates at 2000-3000 cells/well in 100% rgf-MG and cultured in an incubator for up to 15 days. Cultures were fed twice weekly by media exchange. 4 x 5 tiled 10X transmitted light (TL) images were acquired daily on the IXM to survey wells for organoid growth and morphology. Tiled images covering the well together with a single field of view (FOV) image

outlined by the yellow bounding box in the tiled images are presented. For comparison, 10X and 20X images acquired on a stand-alone microscope when the HCCorg-1N organoid was originally established (P1) are presented, together with images of P14 and P11 of the HCCorg-1T and HCCorg-2T PDTOs respectively. Transmitted light FOV images of day 5 and day 15 HCCorg-1N P4, HCCorg-1T P9, and HCCorg-2T P15 cultures are presented (**D**). Scale bars in FOV images represent 200 µm. Representative images from multiple independent experiments are presented.

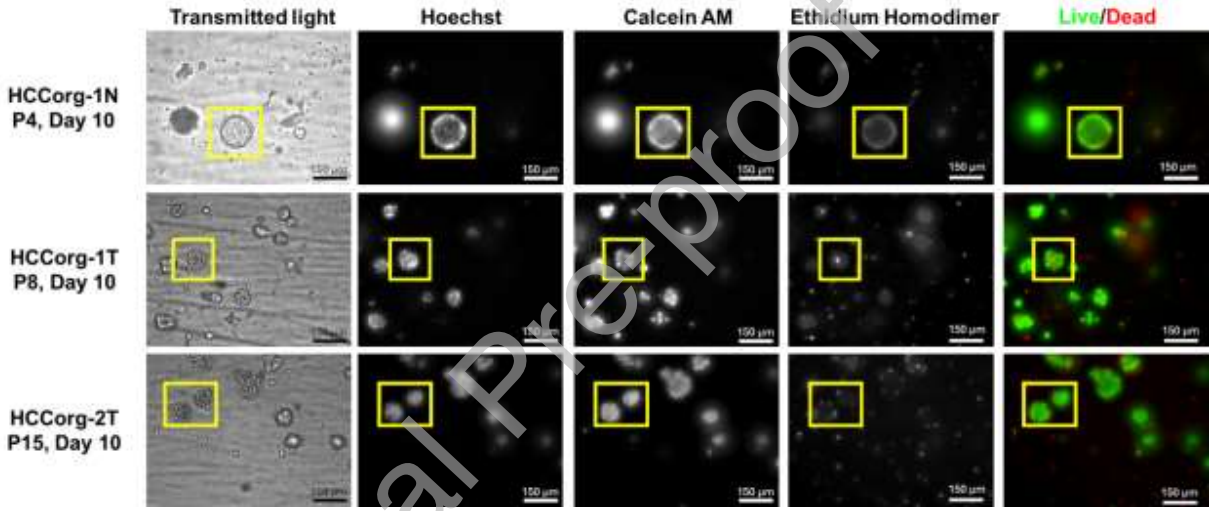

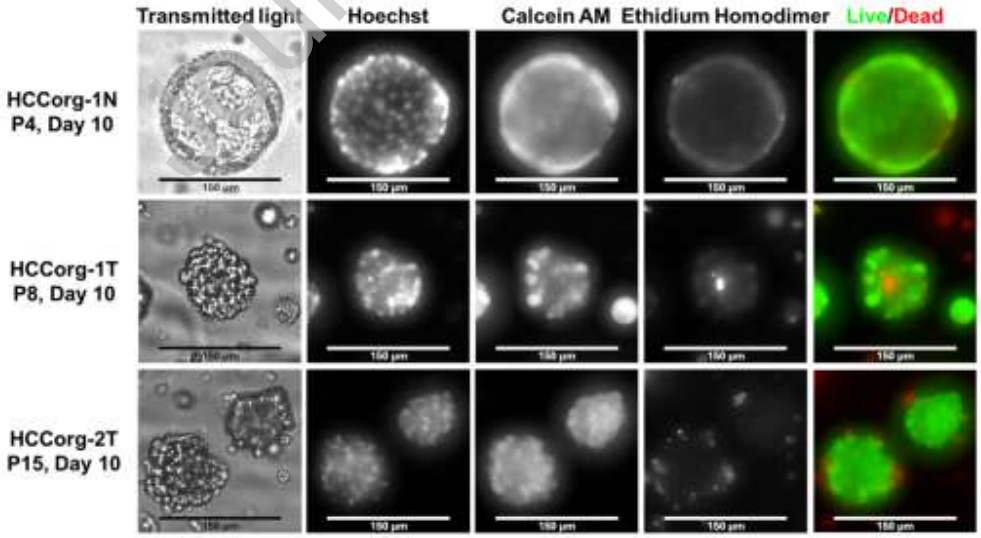

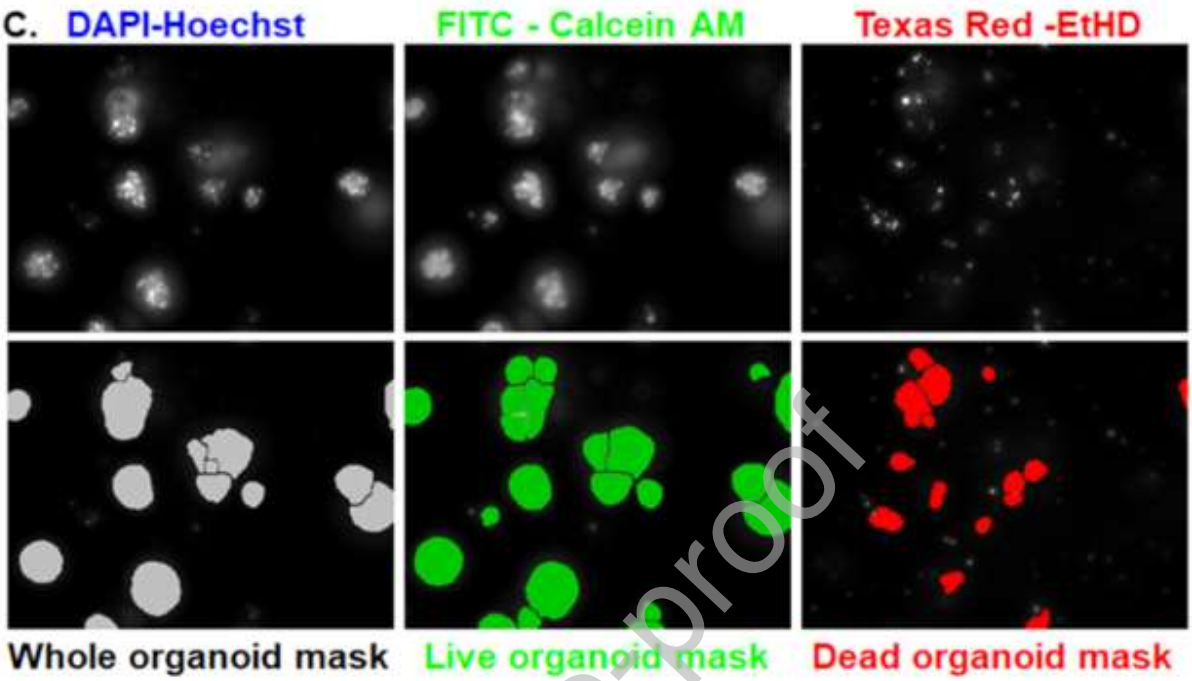

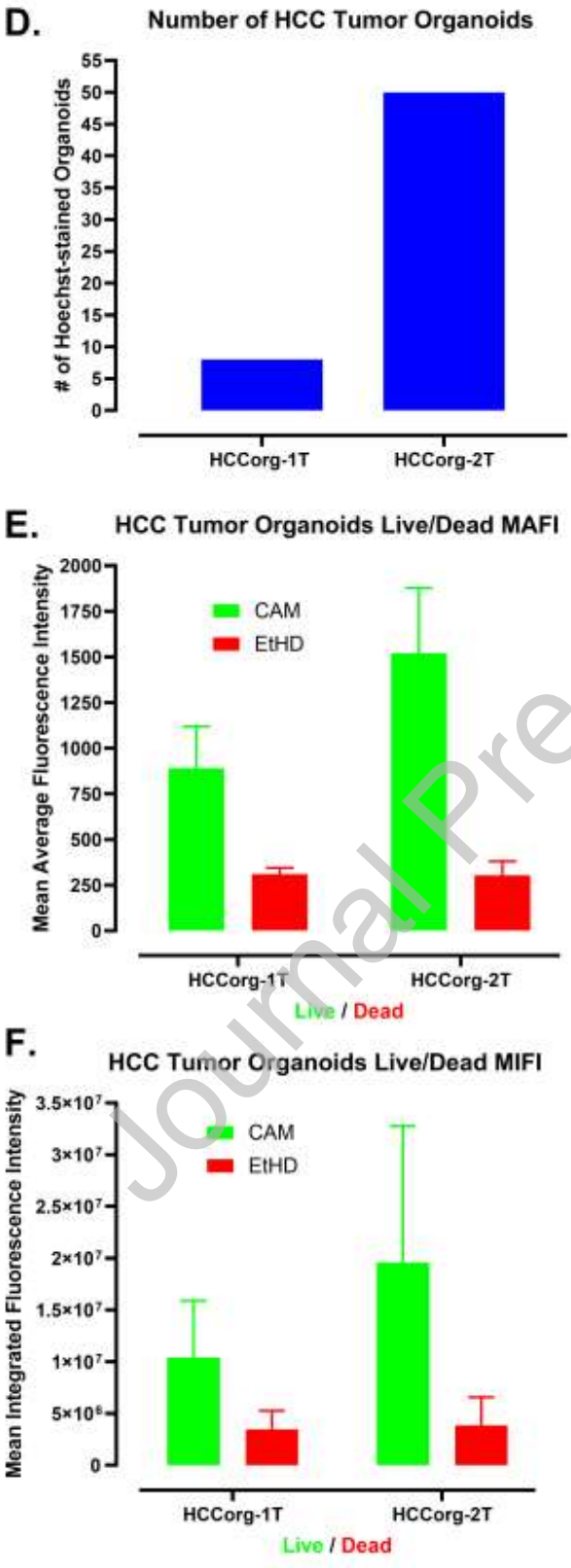

Figure 2. Live/Dead Staining of HCCorg-1N Non-tumor and HCCorg-1T and HCCorg-2T Hepatocellular Carcinoma Organoids cultured in Reduced Growth Factor Matrigel; A) Field of View Images, B) Cropped Images, C) Image Analysis Derived Organoid Masks, D) Number of Hoechst-stained PDTOs, E) Mean Average Fluorescent Intensity of PDTO Calcein AM (CAM) and Ethidium Homodimer (EtHD) Staining, and F) Mean Integrated Fluorescent Intensity of PDTO CAM and EtHD Staining. P4 HCCorg-1N, P8 HCCorg-1T, and P15 HCCorg-2T organoids cultured in 96-well plates for 10 days in 100% rgf-MG were incubated with a cocktail of the Hoechst (8μg/mL), CAM (2.5μM), and EtHD (5μM) reagents for 1h, and images of HCC PDTOs were sequentially acquired on the IXM using either a 4X or 10X objective in both the TL and fluorescent image acquisition modes: DAPI, FITC and Texas Red channels. Full field of view (**A**) and cropped (**B**) 10X TL, Hoechst, CAM, EtHD, and live/dead color composite images are presented. Scale bars in FOV images and corresponding cropped represent 150 μM. We used the multiwavelength cell scoring (MWCS) image analysis module to create organoid masks in the DAPI (grey), FITC (green) and Texas Red (red) channels (**C**). We set the approximate minimum width of the Hoechst-stained nuclei in organoids to be 30 μm with an approximate maximum width to be 200 μm and applied a threshold intensity above local background of 250 grey levels. We then applied background average intensity thresholds, typically 300 and 200 grey levels above local background, for the FITC and Texas Red channels respectfully, and the MWCS image segmentation created total organoid masks in all three fluorescent channels: grey for the DAP1 channel, green for the FITC channels, and red for the Texas red channel. (**C**). The MWCS image analysis module used these masks to quantify the total number of Hoechst-stained organoids (**D**) and the mean average (**E**) and integrated (**F**) fluorescence intensities of the CAM and EtHD signals. Representative images from multiple independent experiments are presented. The MAFI and MIFI data for HCCorg-1T (n=8) and HCCorg-2T (n=50) organoids are presented as the mean ± SD.

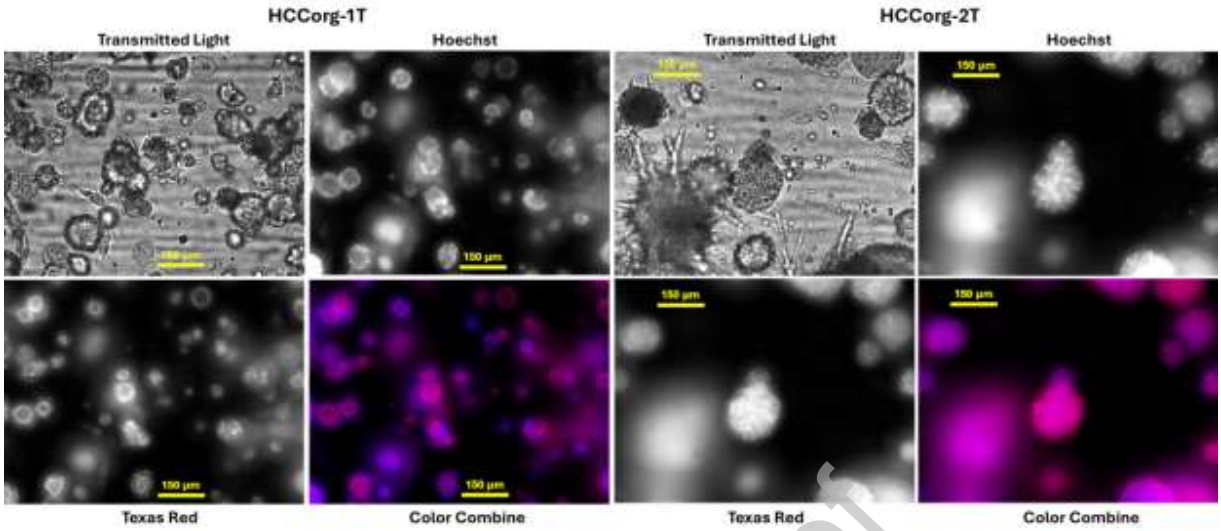

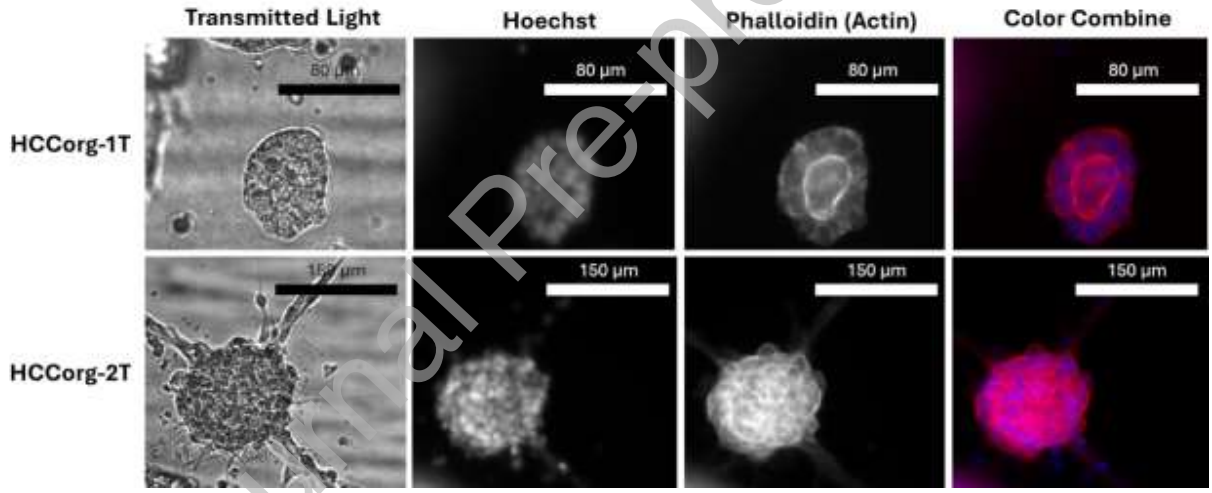

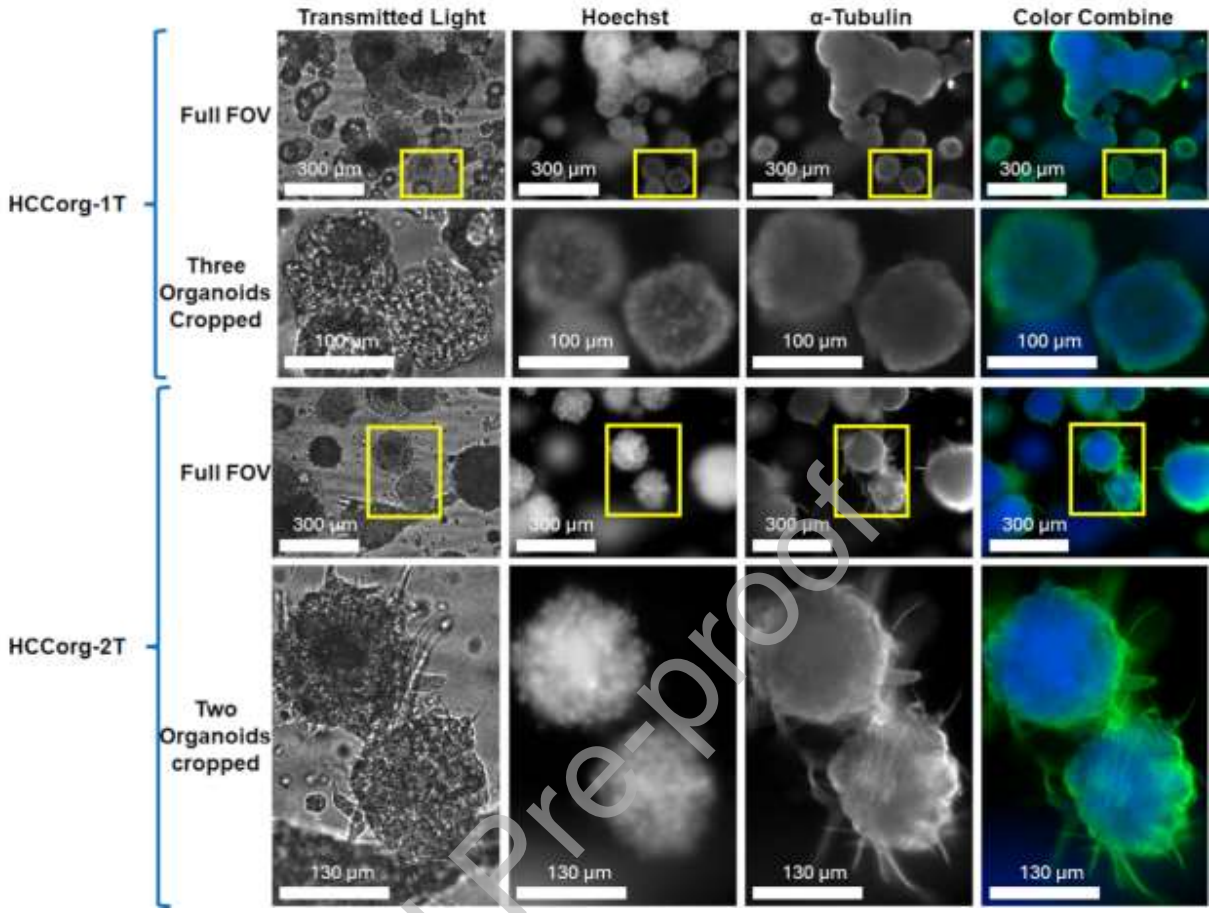

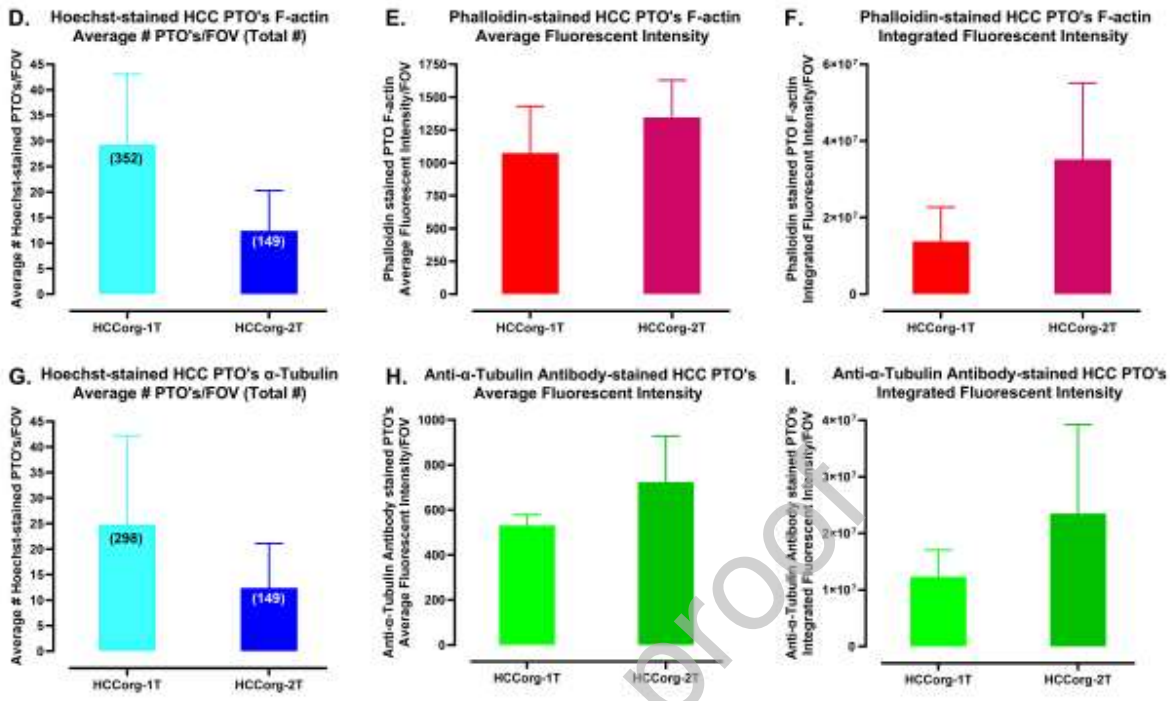

Figure 3. Images and Quantitative data of Phalloidin and Anti-α-Tubulin Antibody Staining of the F-actin and Microtubule Cytoskeletons in of HCCorg-1T and HCCorg-2T Hepatocellular Carcinoma Organoids cultured in Reduced Growth Factor Matrigel; A) Field of view images of Phalloidin stained F-actin, B) Cropped images of Phalloidin stained F-actin, C) Field of view and Cropped images of Anti-α-Tubulin Antibody Stained Microtubules, D) Number of Hoechst-stained PDTOs stained with phalloidin, E) Mean Average Fluorescent Intensity of Phalloidin Staining, F) Mean Integrated Fluorescent Intensity of PDTO Phalloidin staining, G) Number of Hoechst-stained PDTOs stained with α-Tubulin Antibodies, H) Mean Average Fluorescent Intensity of α-Tubulin Antibody Staining, I) Mean Integrated Fluorescent Intensity of PDTO α-Tubulin Antibody Staining. HCCorg-1T and HCCorg-2T organoids cultured in 100% rgf-MG in 96-well plates for 10 days were fixed with formaldehyde and stained with Hoechst, permeabilized overnight (16 h), blocked for 60 min in 1% BSA , and then incubated with Texas Red-X Phalloidin for 16 h at 4°C. 10X images were sequentially acquired on the IXM in the TL, DAPI, and Texas Red

channels. Full field of view (**A**) and cropped (**B**) images of phalloidin stained F-actin are presented. Cropped enlarged images showcase one or two organoids selected from full FOV images. Representative images from multiple independent experiments are presented. Scale bars represent 150 µm in FOV images of HCCorg-1T and HCCorg-2T organoids (**A**), and 80 µm and 150 µm in cropped images of HCCorg-1T and HCCorg-2T organoids respectively (**B**). To stain microtubules (**C**), organoids were fixed, stained with Hoechst, permeabilized , and blocked with 0.1% Tween-20. Organoids were then incubated with a 1:1000 dilution of α-Tubulin mouse monoclonal primary antibody (mAb) at 4°C for 16 h. After washing in, organoids were incubated with a 1:1000 dilution of AlexaFluor-488 conjugated goat anti-mouse antibody for 2 h at room temperature. After washing images of HCC organoids were sequentially acquired on the IXM using a 10X objective in the TL, DAPI, and FITC fluorescent image acquisition modes. Full FOV and cropped 10X TL, Hoechst, FITC (anti-α-Tubulin), and DNA/α-Tubulin color combined images of HCCorg-1T and HCCorg-2T organoids are presented (**C**). Representative images from multiple independent experiments are presented. Scale bars represent 300 µm in FOV images of HCCorg-1T and HCCorg-2T organoids, and 100 µm and 130 µm in cropped images of HCCorg-1T and HCCorg-2T organoids respectively (**C**). The MWCS whole organoid image analysis algorithm was utilized to quantify the number of Hoechst-stained HCCorg-1T and HCCorg-2T organoids analyzed (**D & G**) and the relative average (**E & H**) and integrated (**F & I**) fluorescent intensities of the phalloidin-stained F-actin (**D, E, & F**) anti-α-Tubulin antibody stained microtubule (**G, H, & I**) signals. Quantitative data are presented as the mean ± SD, and representative data from one of two independent experiments are presented.

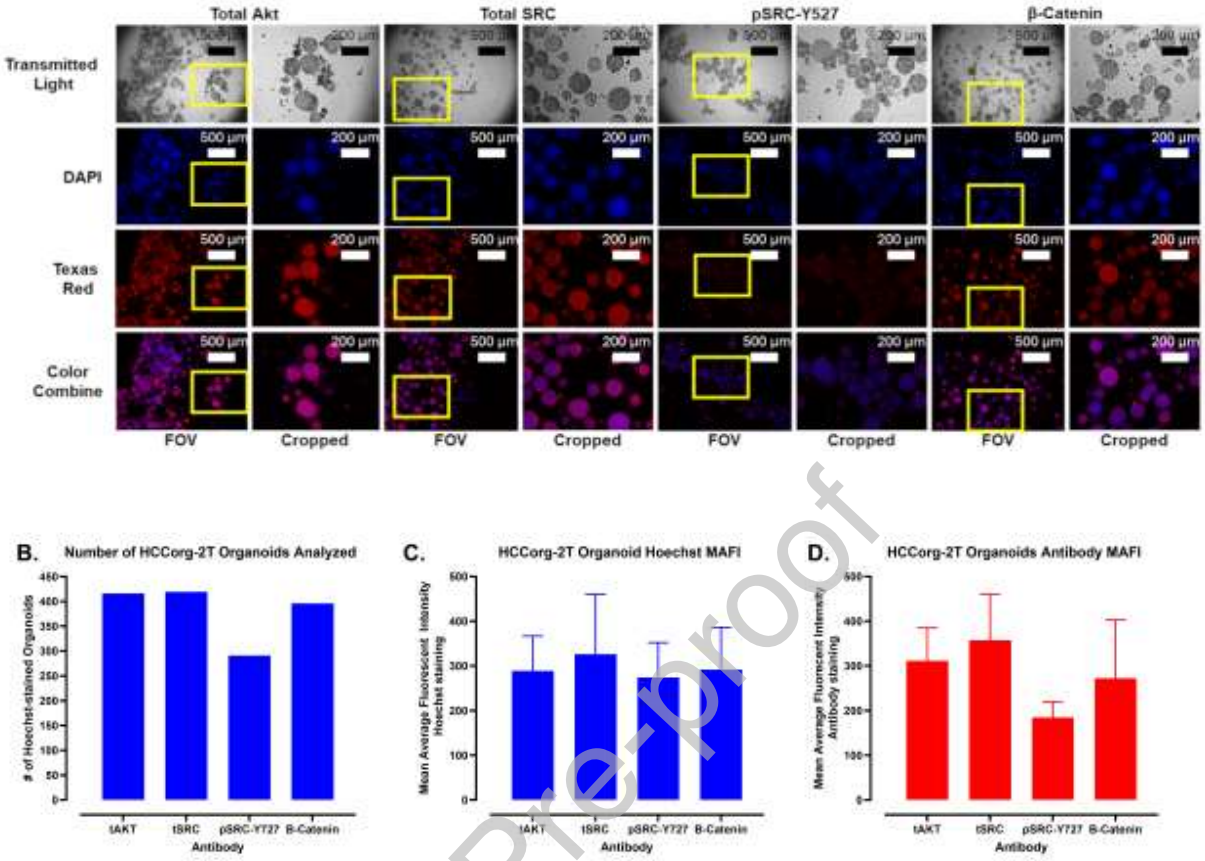

Figure 4. Antibody Staining of Endogenous Signaling Pathway Proteins in HCCorg-2T Hepatocellular Carcinoma Organoids cultured in Reduced Growth Factor Matrigel; A) Field of View and Cropped Images of Endogenous Signaling Pathway Protein Antibody Staining, B) Number of Hoechst-stained Organoids Analyzed C) Mean Average Fluorescent Intensity of Organoid Hoechst DNA Staining, and D) Mean Average Fluorescent Intensity of Organoid Endogenous Signaling Pathway Protein Antibody Staining. Established HCCorg-2T organoids PDTOs that had been cultured in 100% rgf-MG in 96-well plates were fixed and stained with Hoechst, permeabilized overnight (16 h), and organoids were blocked for 60 min in 1% BSA. Organoids were then incubated with a 1:100 dilution of primary antibodies to Akt, Src, pSrc-Y527, or β-Catenin at 4°C for 16 h. After washing organoids were incubated with a 1:1000 dilution of Goat anti-rabbit secondary antibodies

conjugated with Texas Red, washed, and images were sequentially acquired on the IXM using a 10X objective in the TL, DAPI, and Texas Red fluorescent image acquisition modes. Full FOV and cropped images indicated by the yellow bounding boxes, of the TL, Hoechst (blue), Texas Red (Akt, Src, pSrc-Y527, or β-Catenin, red), and DNA/signaling protein color combined images of HCCorg-2T organoids are presented (**A**). Representative images from two independent experiments are presented. Scale bars represent 500 μm in FOV images and 200 μm in cropped images of HCCorg-2T organoids. We used a modified version of the MWCS image analysis module to establish whole organoid masks in the DAPI and Texas red channels and used these to quantify the number of Hoechst-stained organoids analyzed (**B**), the mean average fluorescent intensity (MAFI) of Hoechst DNA staining in organoids (**C**), and the MAFI of endogenous signaling pathway protein antibody staining in organoids (**D**). The MAFI data for Hoechst-stained HCCorg-2T organoid and signaling pathway protein antibody staining are presented as the mean ± SD. The number of HCCorg-2T organoids stained with antibodies for Akt, Src, pSrc-Y527, or β-Catenin were 416, 419, 291, and 396 respectively.

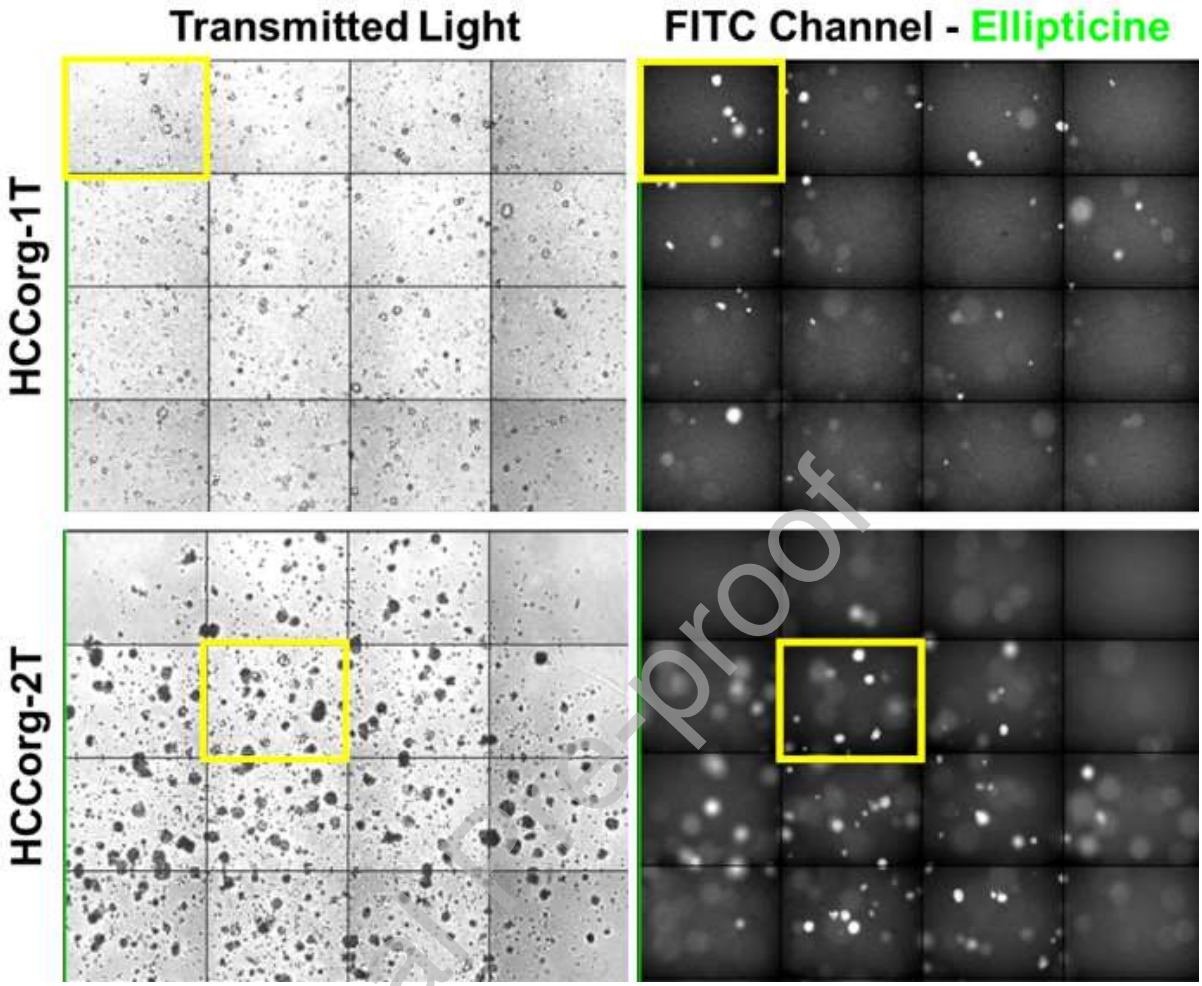

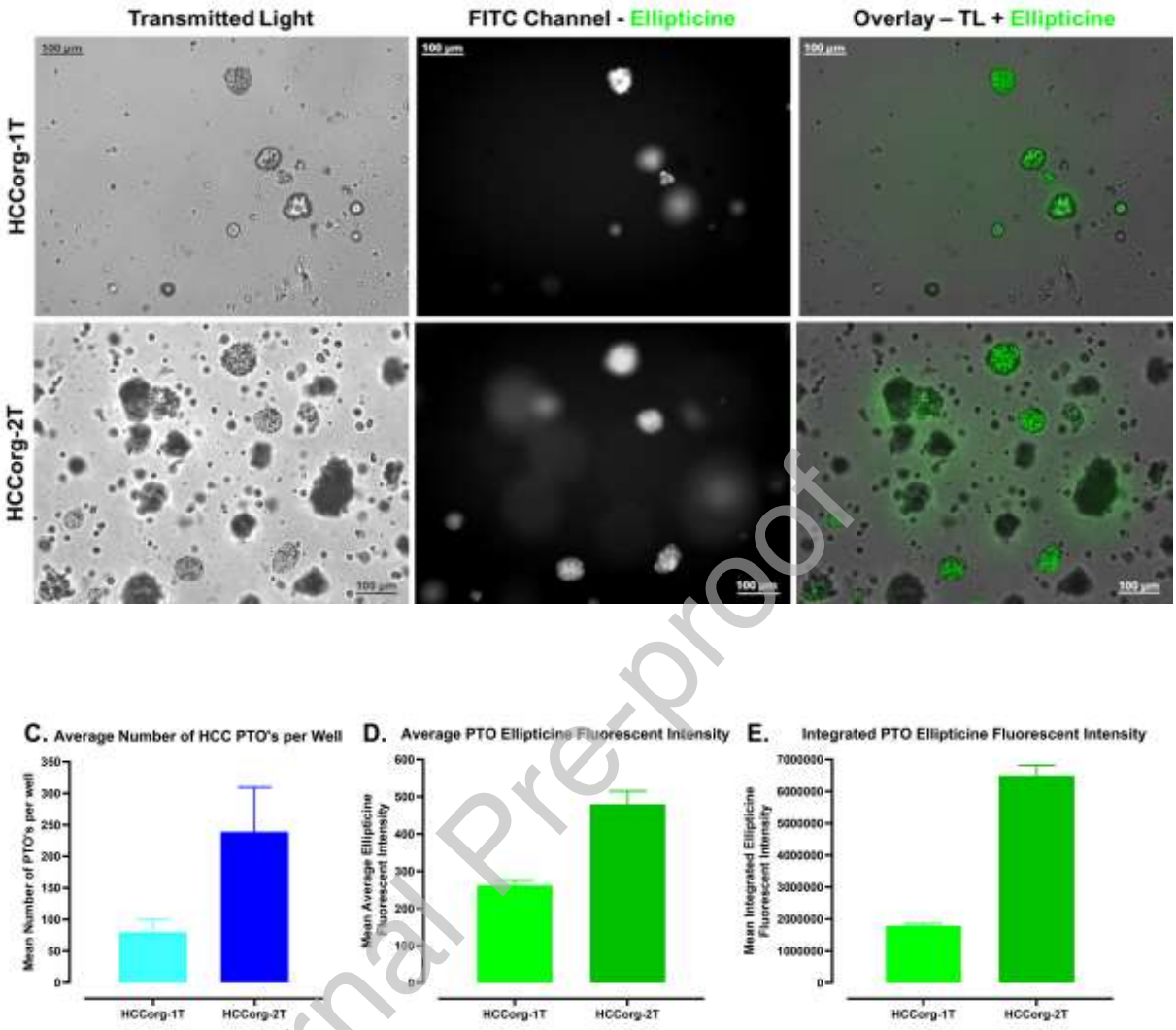

Figure 5. Ellipticine Drug Penetration, Accumulation, and Fluorescent Staining of HCCorg-1T and HCCorg-2T Hepatocellular Carcinoma Organoids cultured in Reduced Growth Factor Matrigel; A) Whole well Tiled Images of Transmitted Light and FITC Channels, B) Individual Field of View and Overlay images of Transmitted Light and FITC channels, C) Number of Hoechst-stained Organoids Analyzed, D) Mean Average Fluorescent Intensity of Organoid Ellipticine Accumulation, and E) Mean Integrated Fluorescent Intensity of Organoid Ellipticine Accumulation. Established HCCorg-1T and HCCorg-2T organoids that had been cultured in 75% rgf-MG in 96-well plates for 15 and 8 days respectively were exposed to 10 µM ellipticine in an incubator for 1 h. 4 x 4 tiled 4X TL and

FITC images of live organoid cultures were then acquired on the IXM to survey the wells for HCC organoid ellipticine accumulation (**A**). Individual 4X FOV TL and FITC images (**B**) outlined by the yellow bounding box in the tiled images are presented together with image overlays of the two channels. Representative images from one of two independent experiments are presented. Scale bars in FOV images represent 100 µm. The MWCS whole organoid image analysis algorithm was utilized to quantify the number of HCCorg-1T and HCCorg-2T organoids analyzed (**C**) and the relative average (**D**) and integrated (**E**) fluorescent intensities of ellipticine accumulation in PDTO's. Quantitative data are presented as the mean ± SD, and representative data from one of two independent experiments are presented.

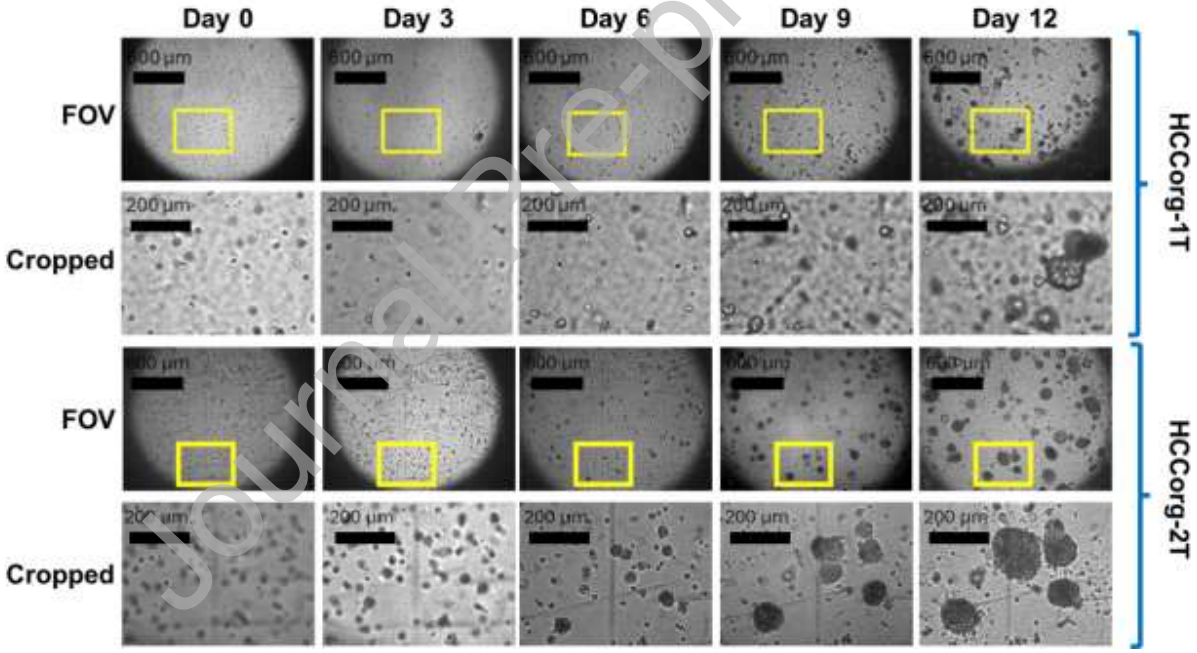

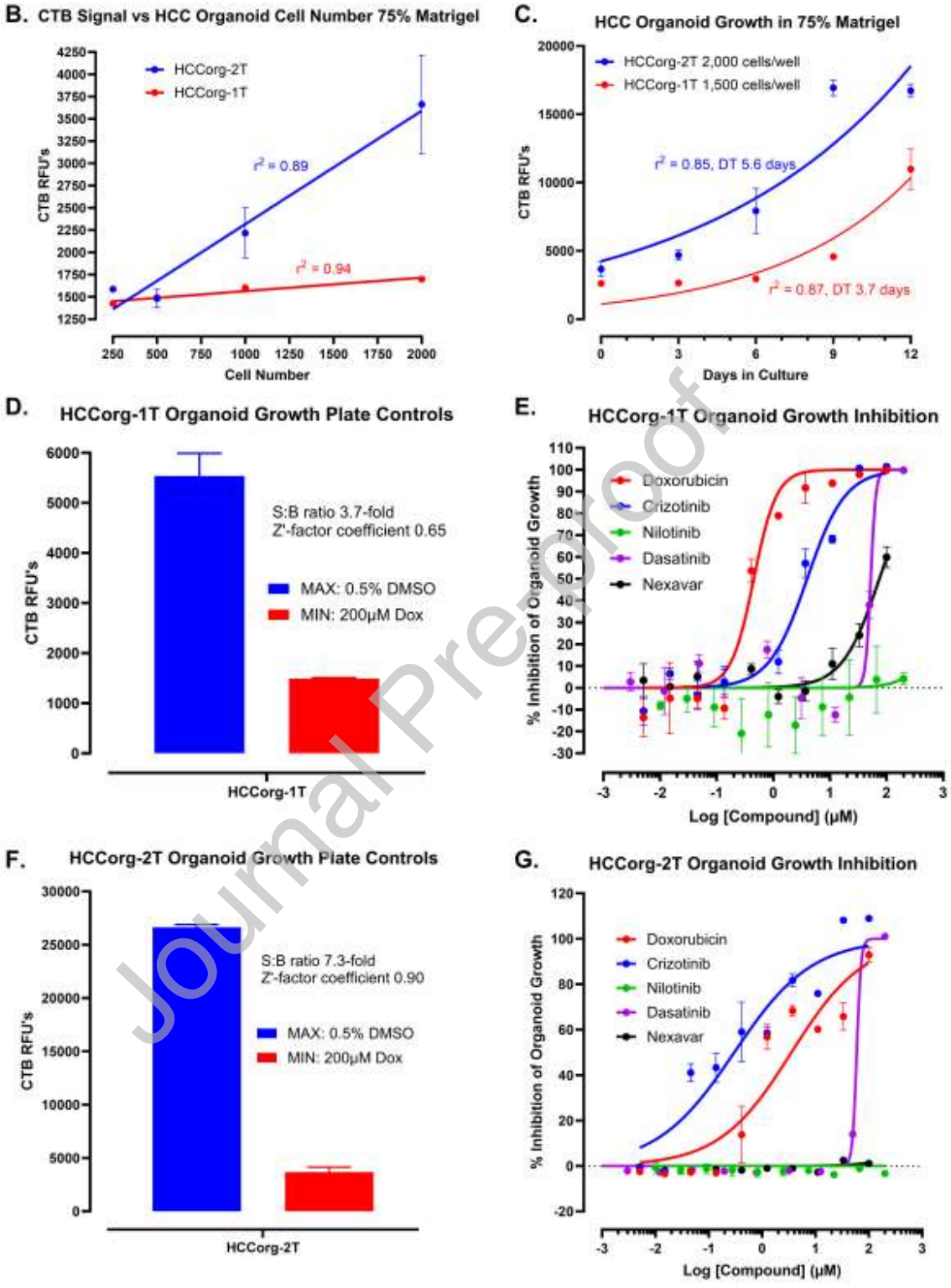

Figure 6. 384-well Growth and Growth Inhibition Assays for HCCorg-1T and HCCorg-2T Hepatocellular Carcinoma Organoids cultured in 75% Reduced Growth Factor Matrigel; A) Sequentially Acquired Transmitted Light Images of HCCorg-1T and HCCorg-2T Organoids, B) Linearity of the Cell Titer Blue (CTB) Signal versus Viable Cell Seeding Density on Day 0, C) Exponential Increase in Organoid CTB Signals with time in culture, D) HCCorg-1T Maximum DMSO (Max) and Minimum Doxorubicin (Min) Assay Plate Controls, E) HCCorg-1T Growth Inhibition Curves, F) HCCorg-2T Max and Min Assay Plate Controls, G) HCCorg-2T Growth Inhibition Curves. HCCorg-1T and HCCorg-2T cells were seeded at 1,500 and 2.000 cells per well in 75% rgf-MG and growth media in 384-well plates and were fed every 3 days by automated media exchange. To assess HCCorg-1T and HCCorg-2T organoid growth and morphologies over time in culture, single 4X TL FOV images were acquired every 3 days and these images are presented together with cropped images of the areas indicated by the yellow bonding box (**A**). To determine whether HCCorg-1T and HCCorg-2T organoids were compatible with 384-well growth assays we conducted cell titer blue (CTB) cell seeding density and time course experiments and the resulting RFU signals were fit to linear regression (**B**) and exponential growth curves (**C**) respectively. To conduct 384-well HCC organoid growth inhibition assays, HCCorg-1T and HCCorg-2T cells were seeded on day 0 in 75% rgf-MG, on day 3 HCC organoids were fed by automated media exchange, on day 6 HCC organoids were fed by automated media exchange and compounds were dispensed into wells at the indicated concentrations, and on day 9 CTB was added to the wells 4 h later the RFU (Ex. 560 nm/ Em. 590 nm) signals were captured on the M5e plate reader. Also on day 6, maximum control wells (Max, n=32) received 5 µL of DMSO (0.5% final) and minimum control wells (Min, n=32) received 5 µL of doxorubicin (200µM plus 0.5% DMSO final) (**D & F**). The mean Max and Min plate control wells represented uninhibited growth and 100% cytotoxicity respectively and were used to calculate assay performance statistics (**D & F**) and to normalize the data from compound treated wells as % inhibition of growth (**E & G**). Representative data

from two independent CTB HCCorg-1T and HCCorg-2T organoid growth inhibition assays are presented. CTB organoid RFUs represent the mean ± SD of three replicates (n=3). GI_{50} data were fit to a non-linear sigmoidal log (inhibitor) vs. normalized response variable slope model using GraphPad 10 software.

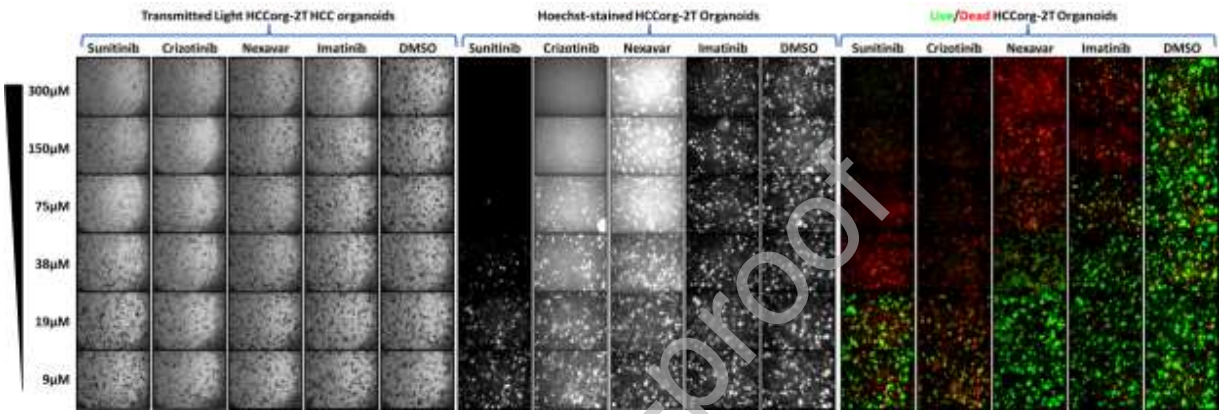

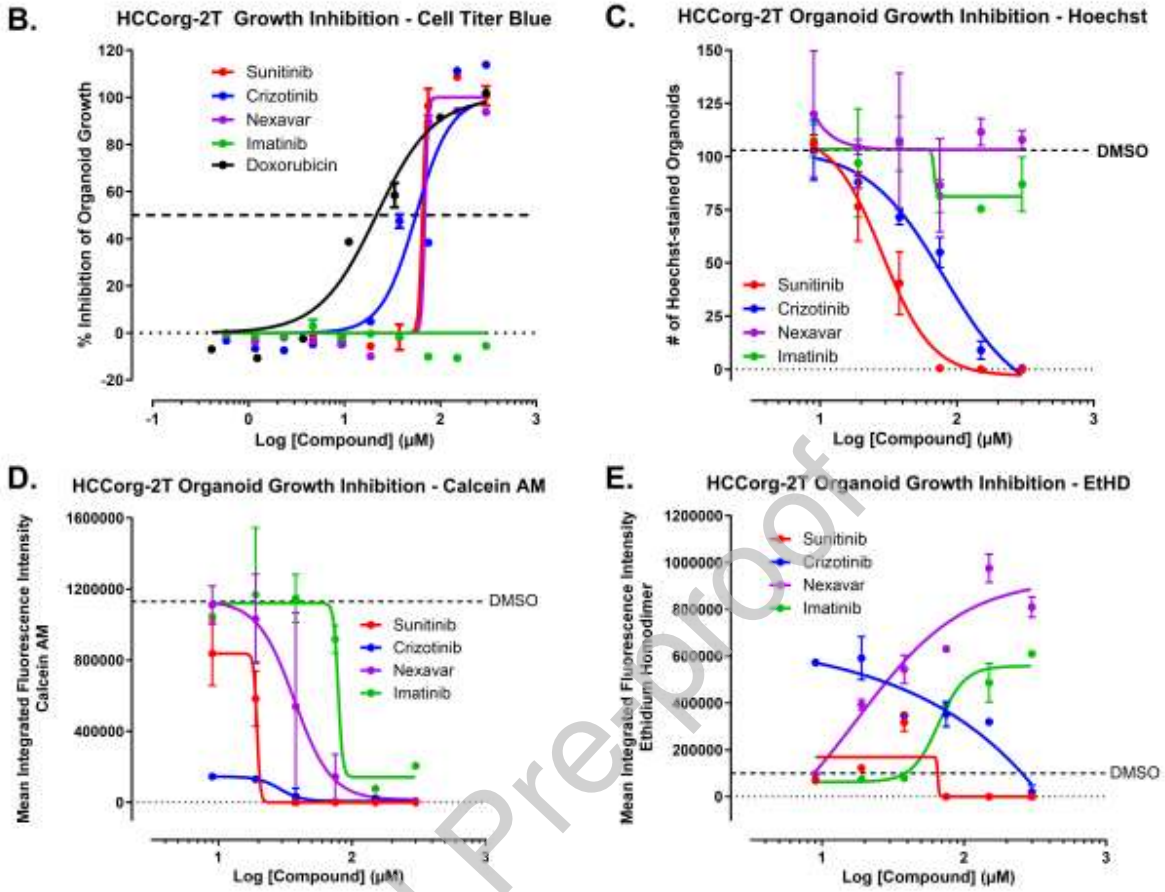

Figure 7. Multiparametric Analysis of 384-well Growth Inhibition Assays for HCCorg-2T Hepatocellular carcinoma Organoids cultured in 75% Reduced Growth Factor Matrigel; A) Whole well organoid montage images of TL and DAPI channels together with color combined FITC (CAM, live, green) plus Texas Red (EtHD, dead, red) channels of compound treated and DMSO controls, B) Cell Titer Blue (CTB) Growth Inhibition Curves, C) Hoechst-stained organoid Growth Inhibition Curves, D) Calcein AM (CAM) live cell Growth Inhibition Curves, and E) Ethidium Homodimer (EtHD) dead cell Growth Inhibition Curves. Additional 384-well growth inhibition assays were conducted in HCCorg-2T organoids to evaluate the impact of 72 h exposure to the TKIs sunitinib, crizotinib, nexavar, and imatinib. Treated HCCorg-2T organoids cultures were stained with a cocktail of Hoechst, CAM and EtHD

and TL, DAPI, FITC and Texas Red channel images were acquired on the IXM. Whole well montage images of the TL and DAPI channels together with color combined FITC (CAM, live, green) plus Texas Red (EtHD, dead, red) channels at six TKI concentrations, ranging from 9 up to 300 µM, plus DMSO controls are shown (**A**). CTB viability measurements were normalized to Max (DMSO) and Min (doxorubicin) plate controls (**B**). The MWCS image analysis module was used to quantify the number of Hoechst-stained organoids (**C**) and the mean integrated fluorescent intensity (MIFI) values of CAM (**D**) and EtHD (**E**) staining. GI_{50} data were fit to a non-linear sigmoidal log (inhibitor) vs. normalized response variable slope model using GraphPad 10 software. Representative data from four independent CTB HCCorg-2T organoid growth inhibition assays are presented. CTB organoid RFUs, number of Hoechst-stained organoids, and organoid CAM and EtHD MIFI data are presented as the mean ± SD of three replicates (n=3).

References:

1. Hait, W. Anticancer Drug Development: the grand challenges. *Nat. Rev. Drug Discovery* **2010,** *9*, 253-254.
2. Hutchinson, L., Kirk, R. High drug attrition rates--where are we going wrong? *Nat Rev Clin Oncol.* **2011,** *8*, 189-190.
3. Ocana, A., Pandiella, A, Siu, LL, Tannock, IF. Preclinical development of molecular-targeted agents for cancer. *Nat Rev Clin Oncol.* **2011,** *8*, 200-209.
4. Sant, S., Johnston, PA. The production of 3D tumor spheroids for cancer drug discovery. *Drug Discov Today Technol.* **2017,** *23*, 27-36.
5. Singh, M., Close, DA, Mukundan, S, Johnston, PA, Sant, S. Production of Uniform 3D Microtumors in Hydrogel Microwell Arrays for Measurement of Viability, Morphology, and Signaling Pathway Activation. *Assay Drug Dev Technol.* **2015** *13*, 570-583.
6. Boehnke, K., Iversen, PW, Schumacher, D, Lallena, MJ, Haro, R, Amat, J, Haybaeck, J, Liebs, S, Lange, M, Schäfer, R, Regenbrecht, CR, Reinhard, C, Velasco, JA. Assay Establishment and Validation of a High-Throughput Screening Platform for Three-Dimensional Patient-Derived Colon Cancer Organoid Cultures. *J Biomol Screen.* **2016,** *21*, 931-941.
7. Colella, G., Fazioli, F, Gallo, M, De Chiara, A, Apice, G, Ruosi, C, Cimmino, A, de Nigris F. Sarcoma Spheroids and Organoids-Promising Tools in the Era of Personalized Medicine. *Int J Mol Sci.* **2018,** *19*.
8. Fong, E., Toh, TB, Yu, H, Chow, EK. 3D Culture as a Clinically Relevant Model for Personalized Medicine. *SLAS Technol.* **2017,** *22*, 245-253.
9. Halfter, K., Mayer, B. Bringing 3D tumor models to the clinic - predictive value for personalized medicine. *Biotechnol J.* **2017,** *12*.

10. Jeppesen, M, Hagel, G, Glenthoj, A, Vainer, B, Ibsen, P, Harling, H, Thastrup, O, Jørgensen, LN, Thastrup, J. Short-term spheroid culture of primary colorectal cancer cells as an in vitro model for personalizing cancer medicine. *PLoS One. 2017 Sep 6;12(9):* **2017,** *12*.
11. Mazzocchi, A., Rajan, SAP, Votanopoulos, KI, Hall, AR, Skardal, A. In vitro patient-derived 3D mesothelioma tumor organoids facilitate patient-centric therapeutic screening. *Sci Rep.* **2018,** *8*.
12. Weeber, F., Ooft, SN, Dijkstra, KK, Voest, EE. Tumor Organoids as a Pre-clinical Cancer Model for Drug Discovery. *Cell Chem Biol.* **2017,** *24*, 1092-1100.
13. Loong HH, W. A., Chan DT, Cheung MS, Chow C, Ding X, Chan AK, Johnston PA, Lau JY, Poon WS, Wong N. Patient-derived tumor organoid predicts drugs response in glioblastoma: A step forward in personalized cancer therapy? *J Clin Neurosci.* **2020,** *78*, 400-402.
14. Broutier L, M. G., Verstegen MM, Francies HE, Gavarró LM, Bradshaw CR, Allen GE, Arnes-Benito R, Sidorova O, Gaspersz MP, Georgakopoulos N, Koo BK, Dietmann S, Davies SE, Praseedom RK, Lieshout R, IJzermans JNM, Wigmore SJ, Saeb-Parsy K, Garnett MJ, van der Laan LJ, Huch M. . Human primary liver cancer-derived organoid cultures for disease modeling and drug screening. . *Nat Med.* **2017,** *23*, 1424-1435.
15. Clevers, H. Modeling Development and Disease with Organoids. *Cell* **2016,** *165*, 1586-1597.
16. Sandro Nuciforo, I. F., Matthias S. Matter, Tanja Blumer, Diego Calabrese, Tujana Boldanova, Salvatore Piscuoglio, Stefan Wieland, Femke Ringnalda, Gerald Schwank, Luigi M. Terracciano, Charlotte K.Y. Ng, Markus H. Heim. Organoid Models of Human Liver Cancers Derived from Tumor Needle Biopsies. *Cell Reports* **2018,** *24*, 1363-1376.
17. Chan, K., Lai, PB, Squire, JA, Beheshti, B, Wong, NL, Sy, SM, Wong, N. Positional expression profiling indicates candidate genes in deletion hotspots of hepatocellular carcinoma. *Mod Pathol.* **2006,** *19*, 1546-1554.
18. Cidon, E. Systemic treatment of hepatocellular carcinoma: Past, present and future. *World J Hepatol.* **2017,** *9*, 797-807.
19. Ge, S., Huang, D. Systemic therapies for hepatocellular carcinoma. *Drug Discov Ther.* **2015,** *9*, 352-362.
20. Ghouri, Y., Mian, I, Rowe, JH. Review of hepatocellular carcinoma: Epidemiology, etiology, and carcinogenesis. *J Carcinog.* **2017,** *16*.
21. Wong, N., Chan, KY, Macgregor, PF, Lai ,PB, Squire, JA, Beheshti, B, Albert, M, Leung, TW. Transcriptional profiling identifies gene expression changes associated with IFN-alpha tolerance in hepatitis C-related hepatocellular carcinoma cells. *Clin Cancer Res.* **2005,** *11*, 1319-1326.
22. Mittal, S., El-Serag, HB. Epidemiology of hepatocellular carcinoma: consider the population. *J Clin Gastroenterol.* **2013,** *47*, S2-6.
23. Torre, L., Bray, F, Siegel, RL, Ferlay, J, Lortet-Tieulent, J, Jemal, A. Global cancer statistics, 2012. *CA Cancer J Clin.* **2015,** *65*, 87-108.
24. Monga, S. β-Catenin Signaling and Roles in Liver Homeostasis, Injury, and Tumorigenesis. *Gastroenterology.* **2015,** *148*, 1294-1310.
25. Zucman-Rossi, J., Villanueva, A, Nault, JC, Llovet, JM. Genetic Landscape and Biomarkers of Hepatocellular Carcinoma. *Gastroenterology.* **2015,** *149*, 1226-1239.
26. Llovet, J., Zucman-Rossi, J, Pikarsky, E, Sangro, B, Schwartz, M, Sherman, M, Gores, G. Hepatocellular carcinoma. *Nat Rev Dis Primers.* **2016,** *2*.
27. Llovet, J., Villanueva, A, Lachenmayer, A, Finn, RS. Advances in targeted therapies for hepatocellular carcinoma in the genomic era. *Nat Rev Clin Oncol.* **2015,** *12*, 408-424.
28. Gho, J., Ip, WK, Chan, KY, Law, PT, Lai, PB, Wong, N. Re-expression of transcription factor ATF5 in hepatocellular carcinoma induces G2-M arrest. *Cancer Res.* **2008,** *68*, 6743-6751.
29. Llovet, J., Ricci, S, Mazzaferro, V, Hilgard, P, Gane, E, Blanc, JF, de Oliveira, AC, Santoro, A, Raoul, JL, Forner, A, Schwartz, M, Porta, C, Zeuzem, S, Bolondi, L, Greten, TF, Galle ,PR, Seitz, JF,

Borbath, I, Häussinger, D, Giannaris, T, Shan, M, Moscovici, M, Voliotis, D, Bruix, J; SHARP Investigators Study Group. Sorafenib in advanced hepatocellular carcinoma. *N Engl J Med.* **2008,** *359*, 378-390.

30. Bruix, J., Qin, S, Merle, P, Granito, A, Huang, YH, Bodoky, G, Pracht, M, Yokosuka, O, Rosmorduc, O, Breder, V, Gerolami, R, Masi, G, Ross, PJ, Song, T, Bronowicki, JP, Ollivier-Hourmand, I, Kudo, M, Cheng, AL, Llovet, JM, Finn, RS, LeBerre, MA, Baumhauer, A, Meinhardt, G, Han, G; RESORCE Investigators. Regorafenib for patients with hepatocellular carcinoma who progressed on sorafenib treatment (RESORCE): a randomised, double-blind, placebo-controlled, phase 3 trial. *Lancet.* **2017,** *389*, 55-66.
31. Lam YK, Y. J., Huang H, Ding X, Wong AM, Leung HH, Chan AW, Ng KK, Xu M, Wang X, Wong N. . TP53 R249S mutation in hepatic organoids captures the predisposing cancer risk. . *Hepatology.* **2023,** *78*, 727-740.
32. Fancher, A., Hua, Y, Camarco, DP, Close, DA, Strock, CJ, Johnston, PA. Reconfiguring the AR-TIF2 Protein-Protein Interaction HCS Assay in Prostate Cancer Cells and Characterizing the Hits from a LOPAC Screen. *Assay Drug Dev Technol.* **2016**.
33. Feng, Z., Kochanek, S, Close, D, Wang, L, Srinivasan, A, Almehizia, AA, Iyer, P, Xie, XQ, Johnston, PA, Gold, B. Design and activity of AP endonuclease-1 inhibitors. *J. Chem. Biol.* **2015,** *8*, 79-93.
34. Johnston, P., Sen, M, Hua, Y, Camarco, D, Shun, TY, Lazo, JS, Grandis, JR. High-content pSTAT3/1 imaging assays to screen for selective inhibitors of STAT3 pathway activation in head and neck cancer cell lines. *Assay Drug Dev Technol.* **2014,** *12*, 55-79.
35. Johnston, P., Sen, M, Hua, Y, Camarco, DP, Shun, TY, Lazo, JS, Wilson, GM, Resnick, LO, LaPorte, MG, Wipf, P, Huryn, DM, Grandis, JR. HCS Campaign to Identify Selective Inhibitors of IL-6-Induced STAT3 Pathway Activation in Head and Neck Cancer Cell Lines. *Assay Drug Dev Technol.* **2015,** *13*, 356-76.
36. Close, D. A.; Camarco, D. P.; Shan, F.; et al. The Generation of Three-Dimensional Head and Neck Cancer Models for Drug Discovery in 384-Well Ultra-Low Attachment Microplates. *Methods Mol Biol* **2018,** *1683*, 355-369.
37. Kochanek, S., Close, DA, Johnston, PA. High Content Screening Characterization of Head and Neck Squamous Cell Carcinoma Multicellular Tumor Spheroid Cultures Generated in 384-Well Ultra-Low Attachment Plates to Screen for Better Cancer Drug Leads. *Assay Drug Dev Technol.* **2019,** *17*, 17-36.
38. Kochanek, S., Close, DA, Camarco, DP, Johnston, PA. Maximizing the Value of Cancer Drug Screening in Multicellular Tumor Spheroid Cultures: A Case Study in Five Head and Neck Squamous Cell Carcinoma Cell Lines. *SLAS Discov.* **2020,** *25*, 329-349.
39. Shan, F.; Close, D. A.; Camarco, D. P.; et al. High-Content Screening Comparison of Cancer Drug Accumulation and Distribution in Two-Dimensional and Three-Dimensional Culture Models of Head and Neck Cancer. *Assay Drug Dev Technol* **2018,** *16*, 27-50.
40. David A Close, P. A. J. Detection and impact of hypoxic regions in multicellular tumor spheroid cultures formed by head and neck squamous cell carcinoma cells lines. *SLAS Discov.* **2022,** *27*, 39-54.
41. Ahn, S., Jang, SJ, Shim, JH, Kim, D, Hong, SM, Sung, CO, et al. Genomic portrait of resectable hepatocellular carcinomas: implications of RB1 and FGF19 aberrations for patient stratification. *Hepatology.* **2014,** *60*, 1972-1982.
42. Kan, Z., Zheng, H, Liu, X, Li, S, Barber, TD, Gong, Z, Gao, H, et al. Whole-genome sequencing identifies recurrent mutations in hepatocellular carcinoma. *Genome Res.* **2013,** *23*, 1422-1433.
43. Schulze, K., Imbeaud, S, Letouzé, E, Alexandrov, LB, Calderaro, J, Rebouissou, S, Couchy, G, Meiller, C, Shinde, J, Soysouvanh, F, Calatayud ,AL, Pinyol, R, Pelletier, L, Balabaud, C, Laurent, A, Blanc, JF, Mazzaferro, V, Calvo, F, Villanueva, A, Nault, JC, Bioulac-Sage, P, Stratton, MR, Llovet,

JM, Zucman-Rossi, J. Exome sequencing of hepatocellular carcinomas identifies new mutational signatures and potential therapeutic targets. *Nat Genet.* **2015,** *47*, 505-511.
44. Totoki, Y., Tatsuno, K, Covington, KR, Ueda, H, Creighton, CJ, Kato, M, et al. Trans-ancestry mutational landscape of hepatocellular carcinoma genomes. *Nat Genet.* **2014,** *46*, 1267-1273.
45. Grantab, R., Sivananthan, S, Tannock, IF. The penetration of anticancer drugs through tumor tissue as a function of cellular adhesion and packing density of tumor cells. *Cancer Res.* **2006,** *66*, 1033-1039.
46. Grantab, R., Tannock, IF. Penetration of anticancer drugs through tumour tissue as a function of cellular packing density and interstitial fluid pressure and its modification by bortezomib. *BMC Cancer* **2012,** *12*.
47. Kerr, D., Kaye, SB. Aspects of cytotoxic drug penetration, with particular reference to anthracyclines. *Cancer Chemother Pharmacol.* **1987,** *19*, 1-5.
48. Minchinton, A., Tannock, IF. Drug penetration in solid tumours. *Nat Rev Cancer.* **2006,** *6*, 583-592.
49. Tannock, I., Lee, CM, Tunggal, JK, Cowan, DS, Egorin, MJ. Limited penetration of anticancer drugs through tumor tissue: a potential cause of resistance of solid tumors to chemotherapy. *Clin Cancer Res.* **2002,** *8*, 878-884.
50. Tredan, O.; Galmarini, C. M.; Patel, K.; et al. Drug resistance and the solid tumor microenvironment. *J Natl Cancer Inst* **2007,** *99*, 1441-54.
51. Sailer B, V., JG, Steinkamp, JA, Darzynkiewicz, Z, Crissman, HA. . Monitoring Uptake of Ellipticine and Its Fluorescence Lifetime in Relation to the Cell Cycle Phase by Flow Cytometry. . *Experimental Cell Research.* **1997,** *236*, 259-267.
52. Dudgeon D, S., SN, Shun, TY, Lazo, JS, Strock, CJ, Giuliano, KA, Taylor, DL, Johnston, PA, and Johnston, PA. . . Characterization and Optimization of a Novel Protein-Protein Interaction Biosensor HCS Assay to Identify Disruptors of the Interactions between p53 and hDM2 . *Assay Drug Dev Technol.* **2010,** *8*, 437-458.
53. Johnston PA, S., SN, Hua, Y, Shun, TY, Lazo, JS, Day, BW. . Development and validation of a high-content screening assay to identify inhibitors of cytoplasmic Dynein-mediated transport of glucocorticoid receptor to the nucleus. . *Assay Drug Dev Technol.* **2012,** *10*, 432-456.
54. Cribbes, S., Kessel, S, McMenemy, S, Jean Qiu , Leo Li-Ying Chan. . A Novel Multiparametric Drug-Scoring Method for High-Throughput Screening of 3D Multicellular Tumor Spheroids Using the Celigo Image Cytometer. . *SLAS Discov.* **2017,** *22*, 547-557.

Table 1. HCCorg-1T and HCCorg-2T Hepatocellular carcinoma Organoid Growth Inhibition 50 (GI_{50}) Values

	HCCorg-1T organoids				HCCorg-2T organoids			
Compound	**GI_{50} µM**	**sd**	**n**	**r^2**	**GI_{50} µM**	**sd**	**n**	**r^2**
Doxorubicin	0.454	0.126	3	0.95	3.55	4.16	3	0.89
Crizotinib	3.97	0.934	3	0.96	0.301	0.159	3	0.89
Nilotinib	>200	NA	3	NA	>200	NA	3	NA
Dasatinib	52.7	NC	3	0.91	59.2	NC	3	0.99
Nexavar	74.9	14.8	3	0.89	>100	NA	3	NA

GI_{50} is the concentration of compound that gives a 50% growth inhibition response halfway between 0% and 100%, sd is the standard deviation of the mean GI_{50}, n is the number of

replicates at each compound concentration, and the r^2 value quantifies the goodness of the curve fit and is 1 when the curve goes through every point. NA = not applicable and NC = not calculable.

Table 2. HCCorg-2T Hepatocellular Carcinoma Organoid Growth Inhibition 50 (GI_{50}) Values by Different Assay Formats

HCCorg-2T organoid Growth Inhibition Assay Format				
Compound	**GI_{50} µM**			**EC_{50} µM**
TKI	**CTB**	**HS-Orgs**	**CAM**	**EtHD**
Sunitinib	65.2	29.5	19.5	NC
Crizotinib	43.7	80.6	<9	NC
Nexavar	64.6	>300	37.1	17.7
Imatinib	>300	>300	79.0	66.2

GI_{50} is the concentration of compound that gives a 50% growth inhibition response halfway between 0% and 100%. EC_{50} is the concentration of compound that gives a 50% increase in dead cell staining response halfway between 0% and 100%. TKI = tyrosine kinase inhibitor. CTB = cell titer blue viability reagent. HS-Orgs = number of Hoechst-stained organoids quantified by the multi-wavelength cell scoring (MWCS) image analysis module. CAM = the mean integrated intensity of the Calcein AM live cell staining quantified by the MWCS image analysis module. EtHD = the mean integrated intensity of the ethidium homodimer dead cell staining quantified by the MWCS image analysis module. NC = not calculable.

Declaration of interests

☒The authors declare that they have no known competing financial interests or personal relationships that could have appeared to influence the work reported in this paper.

☐The authors declare the following financial interests/personal relationships which may be considered as potential competing interests: